Transport properties of single channel quantum wires with an impurity: Influence of finite length and temperature on average current and noise

Fabrizio Dolcini[1], Björn Trauzettel[2], Inès Safi[2], and Hermann Grabert[1]
[1] *Physikalisches Institut, Albert-Ludwigs-Universität, 79104 Freiburg, Germany*
[2] *Laboratoire de Physique des Solides, Université Paris-Sud, 91405 Orsay, France*
(Dated: Received 2 September 2004, published 13 April 2005)

The inhomogeneous Tomonaga Luttinger liquid model describing an interacting quantum wire adiabatically coupled to non-interacting leads is analyzed in the presence of a weak impurity within the wire. Due to strong electronic correlations in the wire, the effects of impurity backscattering, finite bias, finite temperature, and finite length lead to characteristic non-monotonic parameter dependencies of the average current. We discuss oscillations of the non-linear current voltage characteristics that arise due to reflections of plasmon modes at the impurity and quasi Andreev reflections at the contacts, and show how these oscillations are washed out by decoherence at finite temperature. Furthermore, the finite frequency current noise is investigated in detail. We find that the effective charge extracted in the shot noise regime in the weak backscattering limit decisively depends on the noise frequency ω relative to v_F/gL, where v_F is the Fermi velocity, g the Tomonaga Luttinger interaction parameter, and L the length of the wire. The interplay of finite bias, finite temperature, and finite length yields rich structure in the noise spectrum which crucially depends on the electron-electron interaction. In particular, the excess noise, defined as the change of the noise due to the applied voltage, can become negative and is non-vanishing even for noise frequencies larger than the applied voltage, which are signatures of correlation effects.

PACS numbers: 71.10.Pm, 72.10.-d, 72.70.+m, 73.23.-b

I. INTRODUCTION

Transport in Tomonaga-Luttinger liquid (TLL) systems has gained a lot of attraction since the appearance of experimental realizations of TLLs, such as cleaved edge overgrowth quantum wires and single wall carbon nanotubes (SWNTs). However, a quantitative comparison between theory and experiment often suffers from the fact that the interaction parameter g of the TLL is not very well known and does not affect the DC conductance and the shot noise of clean wires attached to Fermi liquid leads. As a hallmark of the TLL model has served the power law dependence of the nonlinear conductance of impure wires with respect to temperature and/or applied voltage, which has been observed in transport measurements in semiconductor quantum wires[1,2] as well as in nanotubes.[3] However, some doubts in the determination of g often remain, since dynamical Coulomb blockade leads as well to a power law when the system is embedded in an ohmic environment.[4] It has been shown recently that both the intrinsic interactions and the environmental resistance enter on equal footing in g.[5] Thus, it is important to have alternative ways to measure g in order to validate the existence of TLL systems in nature.

Crucial ingredients, which have been disregarded in earlier theoretical work on transport in TLLs,[6,7] are the finite wire length and the role of the electron reservoirs. A first step towards a better understanding of such systems has been taken by modelling the reservoirs as one-dimensional non-interacting leads, introducing the inhomogeneous TLL (ITLL) model.[8,9,10] It has been shown that the DC conductance of the ITLL is independent of the electron interaction strength. The analysis of this result has lead to a new phenomenon: a momentum conserving reflection at the contacts due to strong electronic correlations in the wire and their absence in the leads.[8] This effect is similar to the Andreev reflections at a metal-superconductor contact.[11] Apparently, a finite wire behaves as an Andreev-type resonator for plasmon excitations: An electron incident from a contact is transmitted in a series of current spikes, which sum up to the flux of an electron, so that ultimately the incident particle is perfectly transmitted. This dynamics gives rise to nontrivial correlation functions.[11,12,13,14] The ITLL model has also been applied recently to study the effects of the Fermi liquid leads on tunneling from an STM tip into a nanotube.[15] Apart from the ITLL model, the finite length of an interacting quantum wire (QW) is also taken into account in the approach of open boundary bosonization[16]. However, there the wire is taken as a disconnected object with sharp edges.

In the presence of an impurity in the QW, the ITLL model in its standard form[8,9,10] can only be treated perturbatively for weak (or strong) impurity strength. As far as the calculation of the average current is concerned, this problem can in principle be eluded by modelling the presence of non-interacting leads through radiative boundary conditions.[17] These have been combined with methods of refermionization[18] and integrable field theories[19] to obtain the exact current voltage characteristics. The non-perturbative analysis of Refs. [18,19] is restricted, up to now, to an infinitely long wire, and it is currently not clear whether this approach can also be applied to the calculation of current fluctuations. For a finite one-dimensional wire at low energies, an alternative formulation of the radiative boundary conditions in

terms of operators instead of expectation values has been proposed.[20] This approach recovers the quasi-Andreev reflections, and could perhaps also enable a treatment of the noise.[21]

Both the voltage dependence of the differential conductance and the frequency dependence of the spectrum of the noise are expected to provide valuable information on interaction effects in a finite length QW. In Ref. [22] we have determined the nonlinear current-voltage characteristics of a QW with an impurity for the case of zero temperature, taking its finite length explicitly into account through the ITLL model. The $I-V$ characteristics shows interaction-dependent oscillations that are due to interference effects between the Andreev-type reflections at the wire-lead contacts and the backscattering at the impurity site. In the present article, we analyze in detail how these oscillations are modified at finite temperature. For a QW with applied voltage V at temperature T there is now apart from eV and k_BT a third relevant energy scale $\hbar v_F/gL$, where the ballistic frequency v_F/gL is the ratio of the plasmon velocity v_F/g and the length of the wire L. As an important consequence of this new energy scale, the current as a function of T at $V = 0$ and the current as a function of V at $T = 0$ are not simply related to each other by an interchange of eV and k_BT as it is the case in the homogeneous TLL.

The main purpose of the present work, however, is to go beyond the investigation of DC properties of ITLL systems by looking at the finite frequency (FF) current noise. Much of the recent interest in noise comes from the fact that shot noise may allow to determine the effective charge that is backscattered off an impurity in the QW.[23] Due to the dominance of $1/f$ noise at low frequencies, shot noise is never really measured at zero frequency, but only down to the kHz range. This raises the question on the influence of a finite measurement frequency on the shot noise level. This issue has been addressed theoretically for a four-terminal fractional quantum Hall edge state geometry.[24] However, the analysis was restricted to chiral TLLs at zero temperature and infinite system size, which effectively corresponds to a vanishing ballistic frequency v_F/gL. In contrast, as will be shown in the present paper, for non-chiral TLLs the ratio between ω and v_F/gL crucially affects the properties of FF noise. For this reason, it is essential to adopt a model which takes the finite length of the system into account. Here, we address this problem within the ITLL model.

From an experimental point of view, there is an advantage in studying FF noise as compared to the AC conductance. While recent theoretical work[8,20,25] has predicted that the AC conductance exhibits Andreev-type oscillations, the high frequency range of these oscillations cannot easily be explored in experiments. The problem is that the frequency $\omega_{\rm AC}$ of the reservoir potential in AC measurements must be low enough to ensure that inelastic processes are sufficiently efficient to establish quasi-equilibrium distributions as assumed in the theory.[20,25] This means that $\omega_{\rm AC}\tau_{in} \ll 1$, where τ_{in} is the characteristic time for inelastic thermalization processes. However, the frequency ω that appears in the expression of the FF noise derived below is not limited by such assumptions. Furthermore, it is possible to measure FF noise in a DC biased circuit.

In the regime $\omega \ll v_F/gL$, the shot noise of an ITLL system in the presence of a weak backscattering potential has been shown to be given by a g-independent classical Schottky formula $S = 2eI_{\rm BS}$, where $I_{\rm BS}$ is the backscattering current.[26,27] Hence, the shot noise is proportional to the electron charge e. In contrast, in the homogeneous TLL model, the fractional charge extracted from the ratio of the noise and the backscattering current in the weak backscattering limit is given by $e^* = eg$ and thus depends on the interaction parameter g.[28] This has essentially been confirmed in shot noise measurements on fractional quantum Hall edge state devices at filling fraction $\nu = 1/3$.[29,30] However, these systems are described by the chiral TLL model, where right and left movers are spatially separated and the effect of contact electrodes is quite different from the non-chiral case discussed here.

Now, the question arises, if it is possible to observe the fractional charge $e^* = eg$ also in QW realizations such as cleaved edge overgrowth QWs or SWNTs. As we have shown recently[31], at frequencies $\omega \approx v_F/gL$, the effective charge extracted by averaging the FF noise in ITLL systems over a frequency range is indeed the quasiparticle charge $e^* = eg$ and not the electron charge e. The origin of this behavior is easily understood: On the one hand, for $\omega \ll v_F/gL$, the noise probes current correlations on long time scales allowing for a large number of scattering processes (at the impurity and Andreev-type reflections at the boundaries to the leads). Thus, the noise probes the current correlations of the non-interacting leads with a complicated scatterer – the interacting QW and the impurity. On the other hand, in the case $\omega \approx v_F/gL$, intrinsic spectral properties of the QW determine the FF noise. Here, we go beyond the analysis of Ref. [31] by explicitly considering the influence of finite temperature on the equilibrium as well as non-equilibrium current noise of a finite-length QW coupled to electron reservoirs. Our general result for the FF noise of a wire with arbitrary length L describes the crossover between the shot noise results for homogeneous TLL[28] and ITLL systems.[26,27] The observability of the fractional charge backscattered at an impurity in a carbon nanotube has also recently been discussed for a four-terminal setup.[32] However, the Hamiltonian used in Ref. [32] does not take the role of the Fermi liquid leads fully into account and entails a factor of g in the shot noise strength even at $\omega \to 0$ in contrast to the findings in Refs. [26,27].

On the experimental side, there has been considerable progress in the study of FF noise, recently. The FF noise of an electrically driven two-state system has been measured,[33] and the high frequency current noise in a diffusive mesoscopic conductor has been observed.[34] The low frequency regime has also been explored experimentally: Shot noise has been measured in bundles of carbon

nanotubes[35] and in SWNT.[36] However, the nature of the system in the former case and the analysis of data in the latter case do not allow to conclude whether the theoretical predictions[26,27] on the shot noise in non-chiral TLL systems have been confirmed or not, so that further work is needed.

The article is organized as follows. In Sec. II, we introduce the ITLL model. Then, in Sec. III, we first discuss the influence of the finite length and electron-electron interactions on the $I-V$ characteristics. Subsequently, in Sec. IV, we present results on the FF noise in ITLL systems and discuss various limits, where we can make contact with earlier work, in particular, the shot noise of the homogeneous TLL model. Finally, we conclude in Sec. V. Technical details are given in the Appendices.

II. MODEL

We model the physical system by the Hamiltonian

$$\mathcal{H} = \mathcal{H}_0 + \mathcal{H}_B + \mathcal{H}_V \,, \tag{1}$$

where $\mathcal{H}_0$ describes the interacting wire, the leads and their mutual contacts, $\mathcal{H}_B$ accounts for the electron-impurity interaction, and $\mathcal{H}_V$ contains the electrochemical bias applied to the wire. Explicitly, we have

$$\mathcal{H}_0 = \frac{\hbar v_F}{2}\int_{-\infty}^{\infty} dx \left[\Pi^2 + \frac{1}{g^2(x)}(\partial_x\Phi)^2\right] , \tag{2}$$

$$\mathcal{H}_B = \lambda \cos\left[\sqrt{4\pi}\Phi(x_0,t) + 2k_F x_0\right] , \tag{3}$$

$$\mathcal{H}_V = -\int_{-\infty}^{\infty} \frac{dx}{\sqrt{\pi}}\,\mu(x)\,\partial_x\Phi(x,t) \,. \tag{4}$$

Here, $\Phi(x,t)$ is the standard Bose field operator in bosonization and $\Pi(x,t)$ its conjugate momentum density.[37] Eq. (2) describes the (spinless) ITLL mentioned in the introduction, which is known to capture the physical features of a QW with short-ranged (screened) Coulomb interaction connected to metallic leads through adiabatic contacts. The interaction parameter $g(x)$ is space-dependent and its value is g in the bulk of the wire, 1 in the bulk of the leads, and supposed to change smoothly from 1 to g at the contacts. A schematic view of this model is shown in Fig. 1. The variation of $g(x)$ is assumed to occur within a characteristic smoothing length L_s. The profile of the function $g(x)$ then identifies two energy scales $E_L = \hbar v_F/gL$ and $E_s = \hbar v_F/L_s$, associated with the length L of the wire and the smoothing length L_s. We assume here that $L_s \gg \lambda_F$ where λ_F is the electron Fermi wavelength. Under these conditions, the electron-electron interaction in the bosonized language remains quadratic in the field Φ, and no backscattering term arises at the wire-lead interfaces, as it is expected for adiabatic contacts.

We also consider the situation $L_s \ll L$, so that $E_L \ll E_s$. In this case the QW has a well defined length, as it is typically the case for carbon nanotubes contacted by metallic leads.[38,39,40] The energy scale E_s is then much larger than the relevant energy scales that must be considered to describe the effects of the finite wire length on the average current and the noise. The precise form of the variation of $g(x)$ at the contacts from g to 1 is therefore not physically relevant to our purposes, and it is consistent to simplify the calculations by adopting a step-like function, namely $g(x) = g$ if x is in the wire (i.e. if $|x| < L/2$) and $g(x) = 1$ if x is in the leads (i.e. if $|x| > L/2$), *cf.* Fig. 1. We mention that the behavior at energies of order E_s has been addressed by Kleimann *et al.* in their study of a one-dimensional quantum dot.[41]

The value v_F appearing in Eq. (2), although being of the same order as the (equilibrium) bare Fermi velocity of the system, may not exactly coincide with the latter. Indeed, as customary when adopting a continuum limit of a lattice model, the actual value of v_F can be renormalized by the electron density as well as by the interaction.[42] In a more detailed model of the ITLL, one could also consider the plasmon velocity v as an independent parameter and replace v_F/g by v in Eq. (2).[8,11] Then, one would take the possible renormalization of v by irrelevant processes, such as Umklapp scattering, into account. As our final results are essentially unaffected by such a sophistication of the model, we will stick to the simple ITLL given by Eq. (2) and assume that the relation $v = v_F/g$ describes the interaction dependence of the plasmon velocity.

Eq. (3) is the $2k_F$ backscattering term at the impurity site x_0, and introduces a strong non-linearity in the field Φ. Near the low-energy fixed-point of the model this term represents a relevant perturbation. As mentioned in the introduction, we will consider here the weak backscattering limit, which amounts to treating Eq. (3) as a perturbation. The conditions on the coupling constant λ in order for this perturbative approach to be reliable have been discussed in Ref. [22] and are recalled below. In passing, we mention that impurity scattering also yields a forward scattering term, which has been omitted, because it is unimportant for the transport properties studied below.

Finally, Eq. (4) describes the coupling to the electrochemical bias due to the leads. In most experiments, leads are normal 2D or 3D metals, and a detailed description of them would require the standard Fermi liquid model. However, since we are interested in properties of the *wire*, such a detailed description of the leads would in fact be superfluous. One can account for their main effect, the applied bias voltage at the contacts, by treating them as non-interacting systems ($g = 1$), as mentioned above. The only essential properties originating from the Coulomb interaction that one needs to retain are i) the possibility to shift the band-bottom of the leads, and ii) electroneutrality in the leads.[27]

Therefore, the function $\mu(x)$ appearing in Eq. (4), which describes the externally tunable electro-chemical

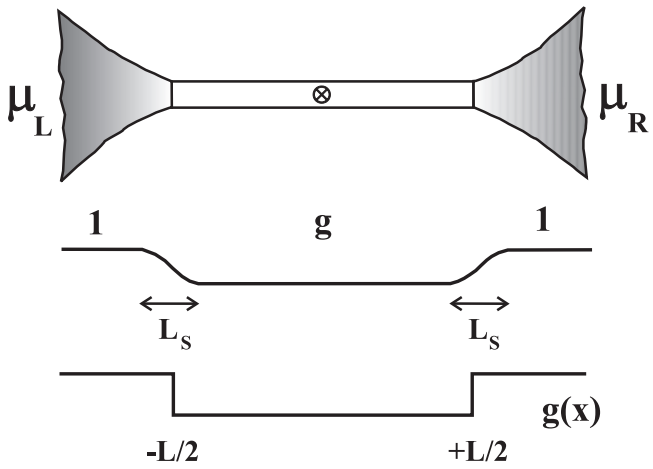

FIG. 1: The upper part of the figure shows a QW with an impurity adiabatically coupled to Fermi liquid leads. In order to allow for a finite bias, the leads are held on different electro-chemical potentials μ_L and μ_R. The middle part of the figure shows the actual variation of the TLL parameter g along the wire-leads system in the ITLL model, and the lower part of the figure its simplification under the assumption that $\lambda_F \ll L_s \ll L$.

bias, is taken as piecewise constant[11]

$$\mu(x) = \begin{cases} \mu_L & \text{for } x < -\frac{L}{2} \\ 0 & \text{for } |x| < \frac{L}{2} \\ \mu_R & \text{for } x > +\frac{L}{2} \end{cases} \tag{5}$$

corresponding to an applied voltage

$$V \doteq (\mu_L - \mu_R)/e \, . \tag{6}$$

We recall that in the absence of the non-linear term (3), the current turns out to be exactly linear with respect to the applied voltage V (see e.g. Ref. [8]).

In bosonization, the current operator is related to the Bosonic field Φ through

$$j(x,t) = \frac{e}{\sqrt{\pi}} \partial_t \Phi(x,t) \, . \tag{7}$$

The finite frequency noise $S(x,y,\omega)$ is defined as

$$S(x,y,\omega) = \int_{-\infty}^{\infty} dt e^{i\omega t} \langle \{\Delta j(x,t), \Delta j(y,0)\} \rangle \ , \tag{8}$$

where $\{\,,\,\}$ denotes the anticommutator and $\Delta j(x,t) = j(x,t) - \langle j(x,t) \rangle$ is the current fluctuation operator.

III. FINITE LENGTH EFFECTS IN THE CURRENT VOLTAGE CHARACTERISTICS

In order to understand the behavior of current fluctuations, especially in the shot noise limit, it is crucial to first provide a thorough description of the average current. As already mentioned above, some results on the current at $T = 0$ have been published previously.[22] In the present section we shall summarize these results, and, in addition, generalize them to the case of finite temperature.

Since we explicitly take into account the finite wire length L, an additional energy scale comes into play, namely the ballistic frequency

$$\omega_L = v_F / gL \tag{9}$$

of the plasmonic excitations in the wire. The average value of the current may be written as $I = I_0 - I_{\rm BS}$, where I_0 is the current the system would exhibit in the absence of the impurity, and $I_{\rm BS}$ is the backscattering current. In App. A we show that for arbitrary impurity strength and time-dependent applied voltage the backscattering current takes the form

$$I_{\rm BS}(x,t) = -\frac{\hbar\sqrt{\pi}}{e^2} \int_{-\infty}^{+\infty} dt' \sigma_0(x,t;x_0,t') \, \langle j_B(x_0,t') \rangle_{\rightarrow} \tag{10}$$

Here $\sigma_0(x,t;y,t')$ is the local conductivity of the clean wire (see App. A, Eq. (A27))[8,11,20,25], and $j_B(x_0,t)$ is the "backscattering current operator", defined as

$$j_B(x_0,t) = -\frac{e}{\hbar} \frac{\delta \mathcal{H}_B}{\delta \Phi(x_0,t)} [\Phi + A_0] \, . \tag{11}$$

$A_0(x_0,t)$ is the field shift emerging when one gauges away the applied voltage, as done in App. A. As before, x_0 is the position of the impurity. Finally, $\langle \ldots \rangle_{\rightarrow}$ denotes an average with respect to the Hamiltonian $\mathcal{H}_{\rightarrow} = \mathcal{H}_0[\Phi] + \mathcal{H}_B[\Phi + A_0]$, which includes the shift A_0 as defined in Eq. (A26). In the case of a DC applied voltage V, $A_0(x_0,t)$ only depends on time (see Eq. (A31)). Then, $I_0 = (e^2/h)V$ and $I_{\rm BS}$ are independent of position and time.

Throughout this article we shall mostly deal with the limit of weak backscattering at the impurity. It is well known that in this regime the shot noise is directly proportional to the backscattering current $I_{\rm BS}$. It is thus worthwhile focussing on the latter, rather than on the total current I. We perform a perturbative expansion in the impurity strength λ appearing in Eq. (3). This is well grounded whenever either of the three energy scales eV, $k_B T$, or $\hbar\omega_L$ is much larger than λ.

It can be shown (see App. A, Eq. (A33) for details) that for a DC voltage Eq. (10) reads to leading order in λ

$$I_{\rm BS} = \frac{e\lambda^2}{4\hbar^2} \int_{-\infty}^{\infty} dt \, e^{i\omega_0 t} \sum_{s=\pm} s \, e^{4\pi C_0(x_0,st;x_0,0)} \, , \tag{12}$$

where $\omega_0 = eV/\hbar$ is the characteristic frequency related to the applied voltage V, and $C_0(x_0,t;x_0,0)$ is the correlation function of the bosonic field $\Phi(x,t)$ in the clean system (see Eq. (B5) in App. B), calculated at the impurity

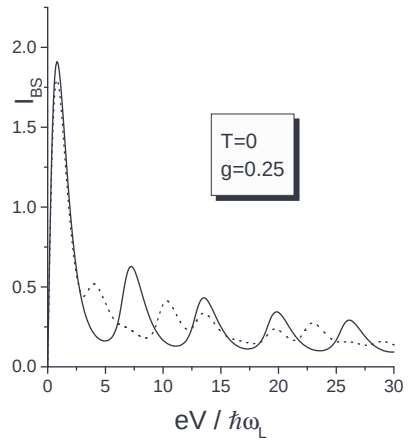

FIG. 2: Behavior of the backscattering current (in units of $e(\lambda\omega_L^g/\omega_c^g)^2/\hbar^2\omega_L$) as a function of V, for two different impurity positions $\xi_0 = 0$ (solid line) and $\xi_0 = \pm 0.2$ (dashed line).

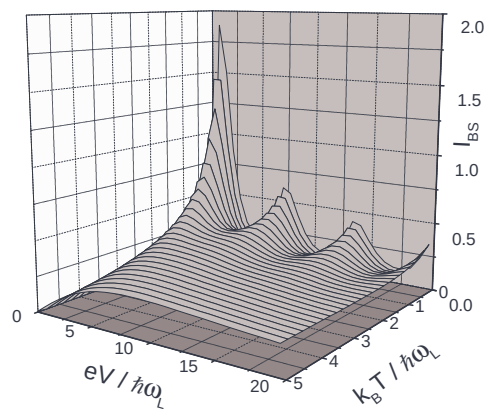

FIG. 3: The backscattering current (same units as in Fig. 2) as a function of voltage and temperature.

position x_0. For arbitrary interaction strength $0 < g \leq 1$, applied voltage V, and temperature T, Eq. (12) can readily be evaluated numerically.

Let us first recall the behavior at $T = 0$.[22] In this case, Eq. (12) for $I_{\rm BS}$ simplifies, because only the term with '$s = +$' contributes, and Eq. (7) of Ref. [22] is recovered. In Fig. 2 we have plotted $I_{\rm BS}$ for the interaction strength $g = 0.25$ (a typical value for SWNTs) and for two different impurity positions, namely $\xi_0 = 0$ and $\xi_0 = \pm 0.2$, where ξ_0 is the *relative* position within the wire, i.e. $\xi_0 = x_0/L$. Notice that the current only depends on the absolute value $|\xi_0|$ of the impurity shift off the center, and not on the direction.

The current exhibits oscillations as a function of the DC voltage V.[22] The origin of these oscillations can be understood from the following two effects: An adiabatic connection between two TLLs with different interaction parameters (in our case g in the wire and 1 in the leads), causes partial reflections of plasmonic excitations at the contact region (Andreev-type reflections); furthermore, in presence of an impurity, an applied DC voltage can be regarded as a time-dependent "phase shifter" located at the impurity site (see the exponential factor $e^{i\omega_0 t}$ in Eq. (12)). This is due to the fact that the applied voltage can be gauged away into a phase factor of the electron operators (see App. A Eqs. (A12), (A20), and (A21) for details).

In view of the above observations one can sketch the following scenario: The plasmonic excitations are backscattered by the impurity, driven towards the contacts where they exhibit further partial Andreev-type reflections, and then come back to the impurity with a phase difference $e^{i\omega_0 t_B}$, where t_B is the ballistic time to propagate from the impurity to one of the contacts and back. This phase difference is responsible for interference effects, which can be tuned from constructive to destructive nature by varying the DC voltage and/or the length of the wire. This is basically the mechanism causing the oscillatory behavior. The typical period of the oscillation of the current as a function of the voltage is indeed $\Delta V = 2\pi\hbar\omega_L/e$. As can be seen from Fig. 2, when the impurity is located away from the middle (i.e $|\xi_0| \neq 0$), the ballistic times to reach the left and right contacts are different, and therefore one observes two different oscillation frequencies as in the dotted curve of Fig. 2.

Importantly, these current oscillations are a combined effect of the impurity, the *finite-length*, and the *interaction* in the wire, which causes the Andreev-type reflections at the contacts. As soon as these reflections are suppressed (either because the interaction in the wire is very weak, or the length is sent to infinity) the oscillations disappear.

Let us now consider the case of finite temperature $T > 0$. Thermal fluctuations are expected to induce decoherence in the interference effects described above. In Fig. 3, the backscattering current $I_{\rm BS}$ is shown as a function of both temperature and voltage, again for the case $g = 0.25$. For simplicity we have chosen an impurity located in the middle, $\xi_0 = 0$. As one can see, when $k_B T$ becomes comparable with the energy scale $\hbar\omega_L$ associated with the ballistic frequency, the oscillations start to be smeared out. Importantly, the existence of a third energy scale $\hbar\omega_L$ (apart from $k_B T$ and eV) destroys the simple scaling behavior of the current as a function of V and/or T known from the homogeneous TLL. More precisely, the current as a function of V at $T = 0$ and the current as a function of T at $V = 0$ behave very differently at intermediate energy scales, *cf.* Fig. 3. The same powerlaws for $I_{\rm BS}(V)$ at $T = 0$ as for $I_{\rm BS}(T)$ at $V = 0$ only arise in the limit $L \to \infty$, i.e. if $eV \gg \hbar\omega_L$ in the former case and $k_B T \gg \hbar\omega_L$ in the latter case.

Fig. 4 shows an interesting behavior of $I_{\rm BS}$ at fixed voltage V as a function of temperature that is due to a combined effect of Andreev-type reflections and temperature induced decoherence. In that figure, we focus on a voltage value $V_{\rm min}$ corresponding to destructive interference at $T = 0$, i.e. to one of the current minima in Fig. 2 (solid curve). If the temperature is increased, one first observes for $k_BT \lesssim \hbar\omega_L$ an increase of $I_{\rm BS}$, due to thermal decoherence of the destructive interference effect. Then, for $k_BT \gg \hbar\omega_L$, $I_{\rm BS}$ decreases, so that a maximum of $I_{\rm BS}$ as a function of T is observed when the voltage is near $V_{\rm min}$.

The above results have been obtained by means of a numerical evaluation of Eq. (12). However, it is also possible to derive analytical results for $I_{\rm BS}$, in particular in the limit $eV \gg \hbar\omega_L$. In this case the two temperature regimes $k_BT \ll \hbar\omega_L$ and $k_BT \gg \hbar\omega_L$ can be distinguished.

(i) In the case $k_BT \ll \hbar\omega_L \ll eV$, it is convenient to rewrite $I_{\rm BS}$ as

$$I_{\rm BS} \,=I^{\rm st}_{\rm BS}(V)\,[1\,+\,f_{\rm BS}(u,\Theta,\xi_0)], \tag{13}$$

where $I^{\rm st}_{\rm BS}$ is the leading order term and $f_{\rm BS}$ gives the corrections. The former reads

$$I^{\rm st}_{\rm BS}(V) = \frac{e^2V}{h}\frac{\pi^2}{\Gamma(2g)}\;\frac{(\lambda/\hbar\omega_c)^2}{(eV/\hbar\omega_c)^{2(1-g)}} \tag{14}$$

and is independent of the length L, of the temperature T, and of the impurity position ξ_0; it exhibits a power law behavior as a function of the applied voltage V, in accordance with the result for the homogeneous TLL.[7] In Eq. (14), ω_c is the high-energy cutoff. As usual, the cutoff dependence can be absorbed in an effective impurity strength $\lambda^* = \hbar\omega_c(\lambda/\hbar\omega_c)^{1/(1-g)}$, in terms of which Eq. (14) reads

$$I^{\rm st}_{\rm BS}(V) = \frac{e^2V}{h}\frac{\pi^2}{\Gamma(2g)}\;\left(\frac{\lambda^*}{eV}\right)^{2(1-g)}. \tag{15}$$

In contrast to the leading order term, the dimensionless correction term $f_{\rm BS}$, which can be evaluated through an asymptotic expansion of Eq. (12), explicitly depends on the length L of the wire, on the temperature T, and on the position of the impurity x_0 through the dimensionless parameters $u = eV/\hbar\omega_L$, $\Theta = k_BT/\hbar\omega_L$, and $\xi_0 = x_0/L$. We find that

$$f_{\rm BS}(u,\Theta,\xi_0) \,=\, f^{\rm osc}_{\rm BS}(u,\Theta,\xi_0) \,+\, \ldots, \tag{16}$$

where $f^{\rm osc}_{\rm BS}$ describes the dominant oscillating correction. For $0 < |\xi_0| < 1/2$ the asymptotic expansion yields

$$f^{\rm osc}_{\rm BS}(u,\Theta,\xi_0) = \frac{2\Gamma(2g)}{\Gamma(g\gamma)}\sum_{s=\pm} D^{(1)}(s|\xi_0|;\Theta)\,\frac{\cos\left[(1-2s|\xi_0|)\,u\,-\,\pi g(1+s\gamma/2)\right]}{u^{2g(1-\gamma/2)}}\,\frac{(1+2s|\xi_0|)^{2g\gamma(1-\gamma-\gamma^2/2)}}{(1-2s|\xi_0|)^{g(2-\gamma)}(16|\xi_0|)^{g\gamma}} \tag{17}$$

with

$$\gamma = \frac{1-g}{1+g} \tag{18}$$

and $D^{(1)}(\pm|\xi|;\Theta)$ is a numerical factor of order unity, explicitly given in Eq. (C1). We mention here that a similar asymptotic expansion has been worked out in Ref. [43], where the crossover from TLL to Fermi liquid behavior has been studied for a tunnel barrier.

Notice that Eq. (17) is singular for $\xi_0 \to 0$. This is actually only a mathematical problem: When the distances of the impurity from the two contacts become equal, pairs of poles in the correlation function merge. The full expression (12) for the current is however perfectly regular, and one can indeed still calculate $f^{\rm osc}_{\rm BS}$ for $\xi_0 = 0$ obtaining

$$f^{\rm osc}_{\rm BS}(u,\Theta,0) = \frac{2\Gamma(2g)}{\Gamma(g\gamma)}D^{(2)}(\Theta)\,\frac{\cos\left[u\,-\,\pi g(1+\gamma)\right]}{u^{2g(1-\gamma)}}, \tag{19}$$

where $D^{(2)}(\Theta)$ is a numerical coefficient of order unity, whose detailed expression is given in Eq. (C4).

(ii) In the regime $\hbar\omega_L \ll \{k_BT, eV\}$, $I_{\rm BS}$ can be well approximated by

$$I_{\rm BS} \;\simeq\; \frac{e}{h}\frac{(2\pi)^{2g}}{2\Gamma(2g)}k_BT\left(\frac{\lambda^*}{k_BT}\right)^{2(1-g)} \times\; \sinh(\frac{eV}{2k_BT})\,|\Gamma(g+i\frac{eV}{2\pi k_BT})|^2. \tag{20}$$

Hence, if $\hbar\omega_L$ is the smallest of all relevant energy scales, the oscillatory dependence of $I_{\rm BS}$ on V disappears, and the current is independent of the length of the wire, and, in particular, of the impurity position. Indeed, in this regime the thermal decoherence time is much shorter than the wire ballistic time; thus, the backscattering by the impurity (occurring in the bulk of the wire) cannot be influenced by the physics at the contacts. The result (20) coincides with the prediction for a homogeneous system (see e.g. Ref. [44]), provided that the voltage is rescaled $V \to gV$. Indeed, it is well known that in the homo-

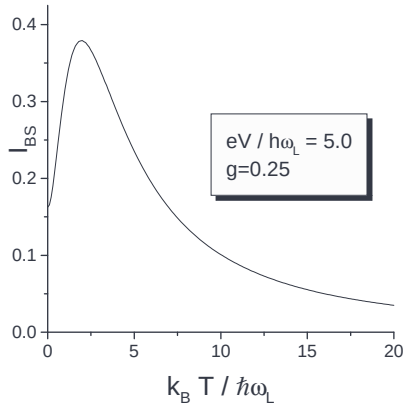

FIG. 4: The backscattering current (same units as in Fig. 2) as a function of temperature, for a voltage value $eV = 5\,\hbar\omega_L$ corresponding to the first current minimum at $T = 0$ in Fig. 2.

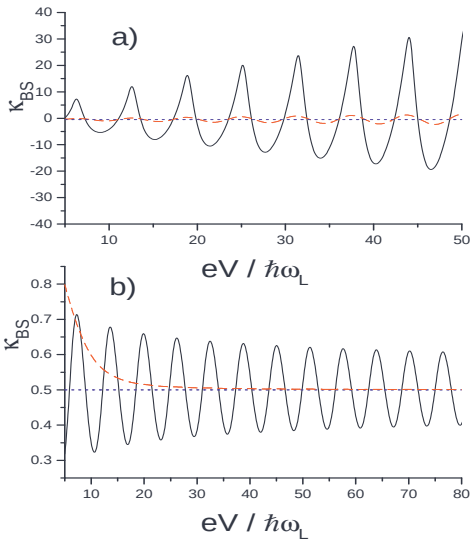

FIG. 5: The dimensionless quantity $\kappa_{\rm BS}(V)$ defined in Eq. (21) as a function of the voltage, for a centered impurity $\xi_0 = 0$: a) shows the case of strong interaction $g = 0.25$, while b) depicts the case of weak interaction $g = 0.75$. The solid lines refer to zero temperature and the dashed lines to the dimensionless temperature $\Theta = k_B T/\hbar\omega_L = 2$. The function $\kappa_{\rm BS}(V)$ oscillates around the value $2g - 1$, indicated by the dotted line, which corresponds to the power law exponent of $I_{\rm BS}$ in the homogeneous TLL model.

geneous TLL an effective voltage gV appears[45], yielding, for instance, an interaction dependent conductance in the case of a clean wire, which is not correct for the system with leads under investigation.[8,9,10] Finally, we mention that when the interaction is switched off ($g \to 1$), the temperature-dependent contribution to $I_{\rm BS}$ in Eq. (20) vanishes by virtue of the identity (B11). This is expected for non-interacting electrons where $I_{\rm BS}$ is a linear function of the applied voltage.

We conclude this section by discussing the behavior of a dimensionless quantity that characterizes the current voltage characteristics

$$\kappa_{\rm BS}(V) = \frac{V}{I_{\rm BS}} \frac{dI_{\rm BS}}{dV} \,. \tag{21}$$

If the wire is assumed to be infinitely long, $I_{\rm BS}$ is simply given by the right-hand side of Eq. (20); in this case, and in particular in the low temperatures regime $k_B T \ll eV$, $\kappa_{\rm BS}$ is actually independent of the voltage and equals $2g - 1$, the power law exponent of $I_{\rm BS}$ in the homogeneous TLL model.
In contrast, for a finite length wire, $\kappa_{\rm BS}$ acquires a non trivial voltage dependence, even at low temperatures. In particular, if $k_B T \lesssim \hbar\omega_L$, $\kappa_{\rm BS}(V)$ exhibits an oscillating behavior around $2g - 1$, due to the Andreev-type reflections discussed previously. An average of $\kappa_{\rm BS}(V)$ over a sufficiently large range of voltages thus allows for an estimate of g from the current-voltage characteristics. Higher temperatures $k_B T \gg \hbar\omega_L$ affect the coherence of the Andreev-type processes, and the amplitude of the oscillations is suppressed. On the other hand, the amplitude of the oscillations also depends on the interaction strength. For the case of a centered impurity, $\kappa_{\rm BS}$ is depicted in Fig. 5, both for strong and weak interaction strength. Interestingly, with increasing voltage the amplitude of the oscillations of $\kappa_{\rm BS}(V)$ increases for strong interaction, and decreases for weak interaction. There is a 'critical' value $g = (1 + \sqrt{17})/8 \simeq 0.64$ at which this change of behavior occurs. This can be determined analytically from the asymptotic expansion (16)-(19) by requiring that the exponent $2g(1 - \gamma)$ of the power law in the denominator of Eq. (19) equals 1.

Fig. 6 refers to the case of an off-centered impurity; in this case the behavior of $\kappa_{\rm BS}(V)$ is characterized by two underlying frequencies ω_{L_1} and ω_{L_2} ($\omega_{L_1} < \omega_{L_2}$), related to the times needed by a plasmon excitation to travel from the impurity to the contacts (see Eq. (17)). Thus, at low temperatures $k_B T \ll \{\hbar\omega_{L_1}, \hbar\omega_{L_2}\}$ the function $\kappa_{\rm BS}(V)$ exhibits two periods. Higher temperatures introduce again decoherence which suppresses the oscillations. However, in the temperature window $\hbar\omega_{L_1} \lesssim k_B T \lesssim \hbar\omega_{L_2}$, only coherence effects related to the Andreev-type reflections from the farther contact will be destroyed, whereas the ones related to the closer contact are only weakly affected. Therefore $\kappa_{\rm BS}(V)$ will exhibit oscillations with one period only. In this regime, a graph of $\kappa_{\rm BS}(V)$ allows to determine: i) the value of g from the average $2g - 1$, and ii) the position of the impurity from the period $\Delta V = \pi\hbar v_F/eg(L/2 - |x_0|)$ of the oscillations as a function of the voltage.

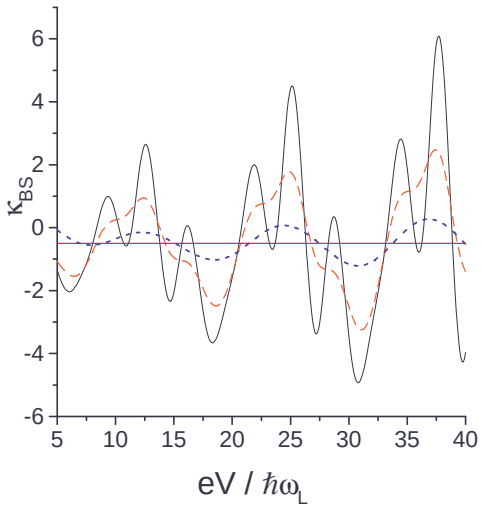

FIG. 6: $\kappa_{\rm BS}(V)$ as a function of the voltage for an off-centered impurity $\xi_0 = 0.25$, and for strong interaction strength $g = 0.25$. The three different curves refer to three different values of the dimensionless temperature $\Theta = k_BT/\hbar\omega_L$: $\Theta = 0.5$ (solid), $\Theta = 1$ (dashed) and $\Theta = 3$ (dotted). The two frequencies mentioned in the text are in this case $\omega_{L_1}/\omega_L = 2/3$ and $\omega_{L_2}/\omega_L = 2$. For low temperatures the voltage dependence is affected by Andreev-type reflections at both contacts. For higher temperatures interference effects only survive for Andreev-type reflections at the closer contact, so that only the frequency ω_{L_2} is present. The average value of the oscillations is $2g - 1$ (horizontal solid line), whereas the period of the oscillations $\Delta V = 2\pi\hbar\omega_L/e(1-2|\xi_0|)$ reveals the position of the impurity.

IV. FINITE FREQUENCY CURRENT NOISE

We now turn to the FF current noise, defined previously in Eq. (8). The noise at finite frequency ω, finite temperature T, finite bias V, and finite length L will be analyzed in the presence of a weak backscatterer in the QW. Mostly, this is done by numerical integration of a general expression derived below. However, analytical results are discussed for the case of thermal equilibrium and for the far from equilibrium shot noise limit, when the applied voltage is much larger than all other relevant energy scales.

A detailed derivation of the full expression for the FF noise in the presence of an impurity is given in App. D. Here, we just mention the final result. In the presence of an impurity, there is a contribution to the noise due to the partitioning of the current at the backscatterer; as a consequence, the noise can be written as

$$S(x,y,\omega) = S_0(x,y,\omega) \, + \, S_{\rm imp}(x,y,\omega)\,, \qquad (22)$$

where the first part, $S_0(x,y,\omega)$, is the current noise in the absence of a backscatterer which will be thoroughly discussed in the following subsection. In contrast, $S_{\rm imp}$ is the supplementary noise due to the impurity, which naturally splits into two parts,

$$S_{\rm imp}(x,y,\omega) = S_A(x,y,\omega) + S_C(x,y,\omega)\,, \qquad (23)$$

namely a contribution $S_A(x,y,\omega)$ related to the Fourier transform of the anticommutator of the backscattering current operator j_B, and a contribution $S_C(x,y,\omega)$ related to the time-retarded commutator of j_B. Notice that, in order to make the notation for S lighter, we have suppressed the temperature T and voltage V arguments, on which the noise depends in general.

The first term in Eq. (23) can be written in a suitable way as

$$S_A(x,y,\omega) \;=\; \frac{1}{4\pi}\left(\frac{h}{e^2}\right)^2 \times \qquad (24)$$
$$\sigma_0(x,x_0,\omega) f_A(x_0,\omega) \sigma_0(x_0,y,-\omega)$$

with

$$f_A(x_0,\omega) = \int_{-\infty}^{\infty} dt\, e^{i\omega t}\, \langle\{\Delta j_B(x_0,t), \Delta j_B(x_0,0)\}\rangle_{\rightarrow}\,, \qquad (25)$$

where $\Delta j_B(x_0,t) = j_B(x_0,t) - \langle j_B(x_0,t)\rangle_{\rightarrow}$. Here, $j_B(x_0,t)$ is the backscattering current operator defined in Eq. (11), while $\sigma_0(x,y;\omega)$ is the local conductivity of the clean system discussed in the following subsection. $S_A(x,y,\omega)$ is the dominant contribution to the noise out of equilibrium, i.e. if $eV \gg \{\hbar\omega_L, \hbar\omega, k_BT\}$. At zero temperature and frequency, $S_A(x,y,\omega)$ is even the only non-vanishing part of the noise and commonly called *shot noise*. The shot noise is independent of the position, as will be demonstrated below.

The second part, $S_C(x,y,\omega)$, is given by Eq. (D15). Using the results in Apps. A and B, it can also be expressed as

$$S_C(x,y,\omega) = \frac{h}{2e^4\omega}\Big\{S_0(x,x_0,\omega) f_C(x_0,-\omega)\sigma_0(x_0,y,-\omega) - S_0(y,x_0,-\omega) f_C(x_0,\omega)\sigma_0(x_0,x,\omega)\Big\} \qquad (26)$$

with

$$f_C(x_0,\omega) = \int_0^{\infty} dt\, \left(e^{i\omega t} - 1\right) \langle[j_B(x_0,t), j_B(x_0,0)]\rangle_{\rightarrow}\,. \qquad (27)$$

In the following subsections we discuss the equilibrium noise, the non-equilibrium noise, and their difference, the

excess noise.

A. Equilibrium noise

1. Equilibrium noise in the clean system

In the absence of a backscatterer, the noise is just given by the first term S_0 of Eq. (22). $S_0(x,y,\omega)$ is directly connected to the Fourier transform of the anticommutator $\tilde{\mathcal{C}}_0^K(x,y,\omega)$ of the bosonic phase field $\Phi(x,t)$ (see Eq. (D13)). The properties of the correlation function (B4) at finite temperature allow to relate S_0 also to the conductivity through the relation[46]

$$S_0(x,y,\omega) = 2\hbar\omega \coth\left(\frac{\hbar\omega}{2k_BT}\right) \Re[\sigma_0(x,y,\omega)]\,, \qquad (28)$$

where $\Re$ denotes the real part. The latter equation is known as the fluctuation-dissipation theorem (FDT). For its derivation, we used that the conductivity can be expressed through the retarded correlation function by the Kubo formula

$$\sigma_0(x,y,\omega) = \frac{2e^2}{h}\omega\tilde{C}_0^R(x,y,\omega)\,, \qquad (29)$$

where $\tilde{C}_0^R(x,y,\omega)$ is given by Eq. (A17) in combination with Eq. (B6). Eq. (28) holds for $x=y$ in general, and also for $x\neq y$ if the unperturbed Hamiltonian preserves time-reversal symmetry, as in our case. The relation (28) holds for any temperature T, noise frequency ω, and system size L. This means that the information that can be gained from the equilibrium noise is fully contained in the AC conductivity. Notice that, by its definition (29), the AC conductivity $\sigma_0(x,y,\omega)$ is voltage independent. Moreover, it can easily be shown to be also temperature independent. This is a direct consequence of the fact that the model Hamiltonian $\mathcal{H}_0$, Eq. (2), which describes an interacting QW without impurity, is quadratic in the boson fields (see App. B for details). Thus, in the absence of a backscatterer, the only temperature dependence of the noise comes from the factor $\coth(\hbar\omega/2k_BT)$ in Eq. (28). In order to determine S_0, we are left with the analysis of the x, ω, and L dependence of the real part of the AC conductivity.

At very high frequencies, the FF noise becomes sensitive to its point of measurement[47], therefore, it is important to discuss for which range of measurement positions the results of our model will be reliable. As described in Sec. II, we model the electron reservoirs by non-interacting one-dimensional QWs. This is legitimate as long as we are not more than an inelastic scattering length l_{in}^R away from the contacts. l_{in}^R is the typical length scale at which inter-channel scattering occurs in the reservoirs. Importantly, l_{in}^R is not necessarily of the same magnitude as the inelastic scattering length in the wire l_{in}^W, which, of course, has to be larger than L, in order to be in the ballistic regime. In some situations, for instance, in cleaved edge overgrowth quantum wires, we expect $l_{in}^R \approx l_{in}^W$, whereas in other situations we expect $l_{in}^R \ll l_{in}^W$, for instance, in carbon nanotubes contacted by gold electrodes.

On the other hand, the model adopts a step-like profile at the contacts for the interaction strength $g(x)$ (see Fig. 1). Therefore, if d_x is the distance between the measurement point (in the lead) and the closer contact, d_x should not be smaller than the smoothing length L_s. Hence, we can state that our model is reliable if the noise is measured at a point x in the range $L_s \lesssim d_x \lesssim l_{in}^R$.

For simplicity, we will now concentrate on the local FF noise, i.e. we will put $x=y$ in Eq. (28). For a point x in one of the leads it can be shown[11] that

$$\sigma_0\left(x,x,\omega\right) = \frac{e^2}{h}\left(1+\gamma\frac{2i\sin(\omega/\omega_L)e^{i2\omega\delta_x/g\omega_L}}{e^{-i\omega/\omega_L}-\gamma^2 e^{i\omega/\omega_L}}\right)\,, \qquad (30)$$

where

$$\delta_x = (|x|-\frac{L}{2})/L = |\xi|-\frac{1}{2} \qquad (31)$$

is the distance d_x, in units of the wire length L. As before, we use the notation $\xi = x/L$ and $\omega_L = v_F/gL$. The real and imaginary parts of Eq. (30) read

$$\Re[\sigma_0\left(x,x,\omega\right)] \;=\; \frac{e^2}{h}\left[1-\sin\left(2\omega\delta_x/g\omega_L\right)h_1(\omega/\omega_L)-\cos\left(2\omega\delta_x/g\omega_L\right)h_2(\omega/\omega_L)\right], \qquad (32)$$

$$\Im[\sigma_0\left(x,x,\omega\right)] \;=\; \frac{e^2}{h}\left[\cos\left(2\omega\delta_x/g\omega_L\right)h_1(\omega/\omega_L)-\sin\left(2\omega\delta_x/g\omega_L\right)h_2(\omega/\omega_L)\right] \qquad (33)$$

with the functions

$$h_1(w) \;=\; \gamma(1-\gamma^2)\frac{\sin(2w)}{1-2\gamma^2\cos(2w)+\gamma^4}, \qquad (34)$$

$$h_2(w) \;=\; \gamma(1+\gamma^2)\frac{1-\cos(2w)}{1-2\gamma^2\cos(2w)+\gamma^4}. \qquad (35)$$

The spatial dependence of the noise follows from Eqs. (28) and (32). In the regime $\omega \ll \omega_L$, the spa-

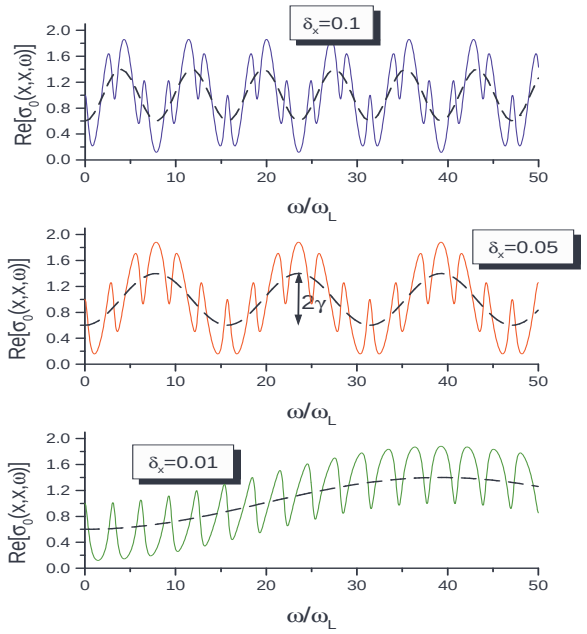

FIG. 7: The real part of the conductivity (32) of a clean wire (in units of e^2/h), is plotted as a function of ω, for three different positions x of the measurement point, and for interaction strength $g = 0.25$; the parameter $\delta_x = (|x| - L/2)/L$ defines the distance of x to the closer contact. One can see the oscillatory behavior characterized by the two periods $\Delta\omega_1$ and $\Delta\omega_2$, with $\Delta\omega_1 \ll \Delta\omega_2$. As the point x gets closer to the contact the beating period $\Delta\omega_2$ tends to infinity. The dashed curve results from an averaging over the rapidly oscillating component with period $\Delta\omega_1$ according to Eq. (38). The oscillation amplitude of the dashed curve is γ, i.e. it allows to determine the interaction strength g from Eq. (18).

tial dependence vanishes. In particular, if $k_BT \gg \hbar|\omega|$, we obtain the thermal or *Johnson-Nyquist noise*

$$S_0(x,x,0) = 4k_BT\frac{e^2}{h}\,, \tag{36}$$

whereas if $k_BT \ll \hbar|\omega|$ we recover the quantum noise or the *zero point fluctuations*

$$S_0(x,x,\omega) = 2\hbar|\omega|\frac{e^2}{h}\,. \tag{37}$$

Hence, if $\omega \ll \omega_L$, the noise does not contain any information about the electron-electron interaction in the finite length QW.

More interesting features appear when ω is comparable or much bigger than the ballistic frequency ω_L. In this regime Eq. (32) is oscillating as a function of ω with two characteristic periods $\Delta\omega_1$ and $\Delta\omega_2$: the former, appearing through $h_{1,2}$, is related to the ballistic frequency $\Delta\omega_1 = \pi\omega_L$; the latter depends on the measurement point and reads $\Delta\omega_2 = \pi g\omega_L/\delta_x$. Typically one has $\Delta\omega_1 \ll \Delta\omega_2$, since $\delta_x \ll 1$; one therefore expects a sort of beating behavior, as shown in Fig. 7 for three different values of x.

The dashed curves represent the function

$$\Re[\sigma_0^{\rm slow}(x,x,\omega)] = \frac{e^2}{h}\left[1 - \gamma\cos(2\omega\delta_x/g\omega_L)\right]\,, \tag{38}$$

obtained by averaging out the fast oscillations, i.e. by replacing the functions $h_{1,2}(\omega/\omega_L)$ in (32) by their average values $\langle h_1\rangle_{\Delta\omega_1} = 0$ and $\langle h_2\rangle_{\Delta\omega_1} = \gamma$, where the averaging is defined as

$$\langle f(\omega/\omega_L)\rangle_{\Delta\omega_1} = \frac{1}{\Delta\omega_1}\int_0^{\Delta\omega_1} f(\omega/\omega_L)d\omega. \tag{39}$$

Interestingly, for any $\delta_x \neq 0$, $\Re[\sigma_0^{\rm slow}(x,x,\omega)]$ in units of e^2/h oscillates around 1 with amplitude γ which is directly connected to the interaction strength g (see Eq. (18)).

For the special case $\delta_x = 0$ (i.e. if one could ideally measure the noise *at the contacts*), Eq. (32) becomes strictly periodic in $\Delta\omega_1$ (the period $\Delta\omega_2 \to \infty$), and the averaging procedure (39) directly yields

$$\Re\left[\sigma_0^{\rm slow}\left(\frac{L}{2},\frac{L}{2},\omega\right)\right] = \frac{e^2}{h}(1-\gamma) = \frac{e^2}{h}g_c\,, \tag{40}$$

where $g_c = 2g/(1+g)$ is the effective TLL interaction parameter at a point contact between a Fermi liquid (with interaction parameter $g = 1$) and a TLL (with interaction parameter g).[8,14]

The frequency dependence of the noise $S_0(x,x,\omega)$, related to $\Re[\sigma_0]$ through Eq. (28), is shown in Fig. 8 for the measurement position $\delta_x = 0.05$ (see Eq. (31)), and for three different values of temperature $\Theta = k_BT/\hbar\omega_L$ ($\Theta = 0, 2, 10$). The noise is shown only for positive ω since S_0 is symmetric in ω by definition. In Fig. 8a one can see that at high frequencies $\omega \gg \omega_L$ the noise exhibits a linear growth modulated by oscillations with period $\Delta\omega_1 = \pi\omega_L$. Fig. 8b is a blow-up of Fig. 8a at small frequencies, showing for $\omega \ll \omega_L$ the Johnson-Nyquist noise (36). Finally, Fig. 8c refers to low temperatures ($\Theta = 0, 0.05, 0.1$) displaying at $T = 0$ and small frequencies the zero-point noise (37).

In the introduction, we have mentioned that in terms of comparison between theory and experiments, it is more suitable to determine $\Re[\sigma_0(x,x,\omega)]$ from a DC noise measurement (through the FDT relation (28)) than from a direct AC conductivity measurement. Here, we have shown that by averaging $\Re[\sigma_0(x,x,\omega)]$ over a frequency range $[0,\pi\omega_L]$ local features of the wire emerge, and the TLL parameter g becomes accessible. This statement will be further supported by the results presented in Sec. IV B.

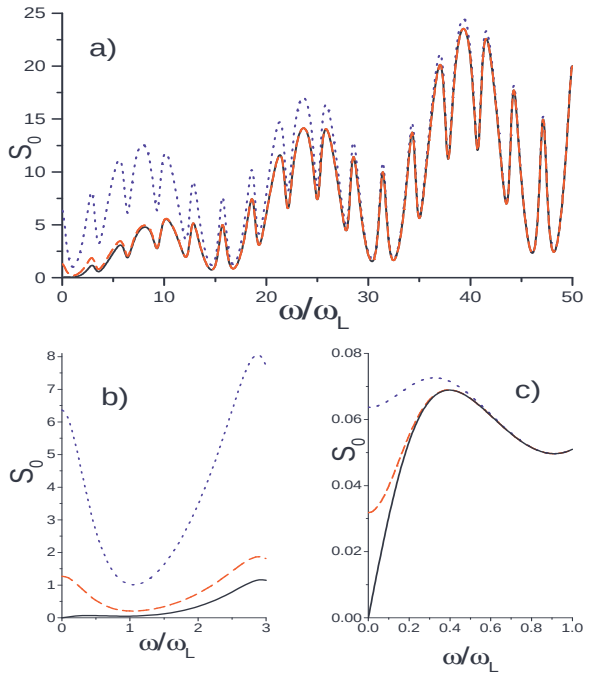

FIG. 8: The noise in the absence of the impurity (in units of $e^2\omega_L$), as a function of ω/ω_L, for the measurement position $\delta_x = 0.05$. a) the whole range of frequencies for three values of the dimensionless temperature $\Theta = k_BT/\hbar\omega_L$ (solid curve $\Theta = 0$, dashed curve $\Theta = 2$, and dotted curve $\Theta = 10$). b) enlargement for the range of low frequencies $\omega \in [0, 3\omega_L]$. c) the case of low temperatures (solid curve $\Theta = 0$, dashed curve $\Theta = 0.05$, and dotted curve $\Theta = 0.1$).

2. *Equilibrium noise in presence of an impurity*

In the presence of an impurity the FDT relating noise S and local conductivity σ still holds. Explicitly one has

$$S(x,y,\omega)|_{V=0} = 2\hbar\omega \coth\left(\frac{\hbar\omega}{2k_BT}\right) \Re[\sigma(x,y,\omega)]|_{V=0}\,, \tag{41}$$

where the general expressions for the conductivity and the noise are provided in App. D (see Eq. (D4) and Eqs. (D12)–(D15), respectively). From Eq. (41) we observe that the noise is real, even for $x \neq y$; this is due to the time-reversal symmetry of the Hamiltonian and the equilibrium condition.

The identity (41) can be verified using Eq. (28) and recalling that *at equilibrium* the following properties hold: (i) the average values $\langle \ldots \rangle_{\rightarrow}$ are evaluated with respect to the Hamiltonian (A26); (ii) $\langle j_B(x_0,t)\rangle_{\rightarrow} = 0$; (iii) the functions f_A and f_C defined in Eqs. (25) and (27) are related by the equation

$$f_A(x_0,\omega)|_{V=0} = 2\coth\left(\frac{\hbar\omega}{2k_BT}\right) \Re\left[\, f_C(x_0,\omega)|_{V=0}\right] \,.$$

Before providing explicit results in the weak backscattering limit, we wish to emphasize two general aspects. First, in contrast to the clean case, in the presence of an impurity the conductivity depends on temperature; as a consequence, the temperature-dependence of the noise is no longer simply given by the coth factor in Eq. (41), and it will be analyzed below.

Secondly, in the static limit $\omega \to 0$, one recovers the relation

$$S(x,y,0)|_{V=0} = 4k_BTG_\lambda \,, \tag{42}$$

where G_λ is the conductance in the presence of the impurity, defined as

$$G_\lambda \doteq \left.\frac{d\langle j(\mathbf{x})\rangle}{dV}\right|_{V=0} \,, \tag{43}$$

which is independent of $\mathbf{x} = (x,t)$ but depends on the temperature T. A direct calculation, using Eq. (D4) in the limit $\omega \to 0$, shows that $G_\lambda = \frac{e^2}{h}(1-\mathcal{R}_\lambda)$, where

$$\mathcal{R}_\lambda = \frac{i}{2e^2}\int_0^\infty dt\, t\ \langle [j_B(x_0,t), j_B(x_0,0)]\rangle|_{V=0} \tag{44}$$

is an effective reflection coefficient. The behavior of $\mathcal{R}_\lambda$ has been analyzed previously.[11,12] It has been shown that, in the regime $k_BT \gg \hbar\omega_L$, $\mathcal{R}_\lambda$ shows a typical TLL powerlaw behavior with respect to the temperature T, recovering the result for the homogeneous TLL.[7] In contrast, in the regime $k_BT \ll \hbar\omega_L$, $\mathcal{R}_\lambda$ shows a powerlaw behavior with respect to the length L of the QW.

In order to prove the relation (42) between the static limit $\omega \to 0$ of the noise S and the conductance G_λ, we have calculated the equilibrium noise from Eqs. (24), (26) and (28), and compared the resulting expression with Eq. (44).

Let us now consider the case of finite frequency. The equilibrium noise can be obtained from the conductivity through Eq. (41). In particular, in the weak backscattering limit an expansion of the conductivity in powers of λ gives to leading order

$$\sigma(x,y,\omega) = \sigma_0(x,y,\omega) + \sigma_{\rm BS}(x,y,\omega) \tag{45}$$

where

$$\sigma_{\rm BS}(x,y,\omega) = -\frac{2}{\hbar\omega}\left(\frac{\pi\lambda}{e}\right)^2 \sigma_0(x,x_0,\omega)\sigma_0(x_0,y,\omega) \times \int_0^\infty dt\,(e^{i\omega t}-1)\left(\sum_{s=\pm} s\, e^{4\pi C_0(x_0,st;x_0,0)}\right). \tag{46}$$

We shall analyze here the local noise $S(x,x,\omega)$ for a point x located in the leads. Comparing Eqs. (41) and (22), one can easily recognize that the first term on the r.h.s. of Eq. (45) yields the noise S_0 of the clean wire, whereas the second term determines the supplementary noise $S_{\rm imp}$ due to the backscattering at the impurity.

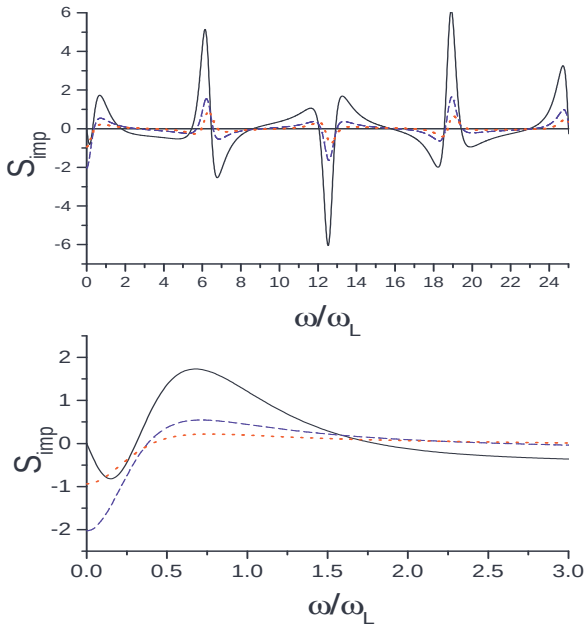

FIG. 9: The impurity noise $S_{\rm imp}$ at equilibrium (in units of $e^2\omega_L(\lambda^*/\hbar\omega_L)^{2(1-g)}$), as a function of ω/ω_L, for the measurement position $\delta_x = 0.05$, the impurity in the center ($\xi_0 = 0$), and three different values of the dimensionless temperature $\Theta = k_BT/\hbar\omega_L$ (solid curve $\Theta = 0$, dashed curve $\Theta = 2$, and dotted curve $\Theta = 10$). Lower graph: Enlargement for low frequencies. Finite temperature influences significantly the slope of the noise near $\omega = 0$.

Since the former has been described in the previous subsection, we shall focus now on the latter. The frequency spectrum of $S_{\rm imp}$ is shown in Fig. 9 for three different values of the dimensionless temperature $\Theta = k_BT/\hbar\omega_L$. The upper graph of Fig. 9 shows that $S_{\rm imp}$ oscillates around $S_{\rm imp} = 0$ with pronounced spikes of either sign, which are washed out when the temperature is increased. While $S_{\rm imp}$ can be negative, the full noise (8) is non-negative. The lower graph of Fig. 9 zooms into the region of low frequencies and illustrates that, at finite temperature, the value of $S_{\rm imp}$ at $\omega = 0$ is negative. This is in accordance with Eq. (42), since the presence of the impurity reduces the conductance G_λ with respect to the clean case.

Fig. 10 shows how the spikes of $S_{\rm imp}$ depend on the position of the impurity. Differently from the average current shown in Fig. 2, the current fluctuations depend not only on the absolute value of the impurity position, but also on the direction of the shift from the center of the wire. This is because in general the noise depends on the measurement point x, which is located in one of the leads, and therefore a shift of the impurity away from the center implies a smaller or bigger distance from the measurement point x.

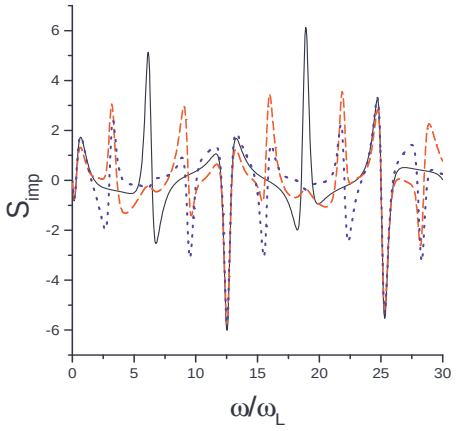

FIG. 10: The zero temperature impurity noise $S_{\rm imp}$ at equilibrium (in units of $e^2\omega_L(\lambda^*/\hbar\omega_L)^{2(1-g)}$) as a function of ω/ω_L, for the measurement position $\delta_x = 0.05$, and interaction parameter $g = 0.25$. Shown are three cases of the impurity position: $\xi_0 = 0$ (solid curve) a centered impurity, $\xi_0 = 0.25$ (dashed curve) an impurity off-centered by 1/4 towards the direction of the measurement point, and $\xi_0 = -0.25$ (dotted curve) an impurity off-centered by 1/4 opposite to the direction of the measurement point.

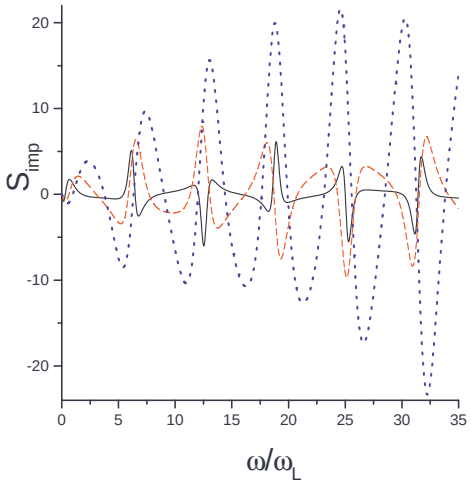

FIG. 11: The zero temperature impurity noise $S_{\rm imp}$ at equilibrium (in units of $e^2\omega_L(\lambda^*/\hbar\omega_L)^{2(1-g)}$) as a function of ω/ω_L, for the measurement position $\delta_x = 0.05$, in the case of a centered impurity ($\xi_0 = 0$) and for three different values of the interaction strength: $g = 0.25$ (solid curve), $g = 0.50$ (dashed curve), and $g = 0.75$ (dotted curve).

The spikes in the spectrum of $S_{\rm imp}$ are essentially due to resonances caused by the Andreev-type reflections at the contacts and backscattering at the impurity. A difference with respect to the clean case should be emphasized: In the clean case the peaks of the conductivity $\sigma_0(x, x, \omega)$ are due to resonant processes where a cur-

rent pulse propagates from the measurement point x and comes back to x after a sequence of Andreev reflections at the contacts. In contrast, in the presence of the impurity, the conductivity $\sigma(x,x,\omega)$ also includes processes, where a current pulse from the measurement point x propagates to the impurity position x_0, and then back from x_0 to the measurement point x, whereby each path segment connecting x and x_0 includes a sequence of Andreev-type reflections. These processes are described by $\sigma_{\rm BS}$ given in Eq. (46), which for $x=y$ contains the product of $\sigma_0(x,x_0,\omega)$ and $\sigma_0(x_0,x,\omega)$. This product is weighted by a time integral over the exponential of the Bose field correlation function at the impurity position, which in turn strongly depends on the interaction strength. As a consequence of this complicated interference of many different contributions, the analytical determination of the location of the peaks of $S_{\rm imp}$ is a complex problem, in which four elementary frequencies combine: $\omega_x = v_F/(|x|-L/2)$, related to the distance of the measurement point from the closest contact, ω_L, the ballistic frequency of the finite length wire, and $\omega_\pm = v_F/g(1/2\pm\xi_0)$ related to the distances of the impurity from the two contacts. A straightforward analytic formula for the peak positions is thus in general not available, however, progress can be made in some limits. For strong interaction ($g \lesssim 0.4$) and in the range of moderate to high frequencies ($\omega \gtrsim 3\omega_L$), the spectrum of $S_{\rm imp}$ is essentially determined by $\Im[\sigma_0^2(x,x_0,\omega)]$. An analysis of this quantity shows that peaks occur at frequencies $\omega = n\pi\omega_L$ (n integer) whenever there is an integer m such that $2n(\omega_x^{-1}\pm\Omega^{-1}) \simeq \omega_L^{-1}(1/2+m)$, where Ω can be either ω_L, ω_+, ω_- or their sums and differences. The peaks are positive (negative) if m is even (odd). Thus, one can realize that for some values of the impurity position, an upward spike due to a resonance with a frequency Ω can be located close to a downward spike related to another frequency Ω', and therefore abrupt changes of the sign of $S_{\rm imp}$ may occur, like in the solid curve of Fig. 10 near $\omega = 2\pi\omega_L$ and $\omega = 8\pi\omega_L$.

On the other hand, for very weak interaction ($g \gtrsim 0.85$) the time-integral in Eq. (46) over the exponential of the Bose field correlation function grows as a power law $|\omega|^{2g-1}$, and therefore plays an important role. At low frequencies $0 < \omega/\omega_L < 10$ one finds that $S_{\rm imp}$ is essentially proportional to $|\omega|^{2g-1}\left(\Re[\sigma_0(x,x_0,\omega)]\right)^2$, which roughly amounts to $S_{\rm imp} \sim |\omega|^{2g-1}\cos^2[\omega(\delta_x/g - 1/2 + \xi_0)/\omega_L]$. The frequency range in which this approximation is valid is however also interaction dependent. In particular, the approximation becomes valid for all frequencies when the interaction is switched off ($g \to 1$). The different forms of the frequency dependence of $S_{\rm imp}$ for various values of the interaction strength g are shown in Fig. 11, where the limiting cases discussed above can be recognized.

B. Non equilibrium noise

Usually the FDT (28) is only valid in thermal equilibrium. However, in the absence of an impurity, the current operator of a QW attached to Fermi liquid leads is a linear superposition of contributions from normal plasmon modes. Since the only mode depending on the voltage (i.e. the zero mode) is noiseless, one can in fact conclude that $S_0(x,x,\omega)$ does not depend on the applied voltage V and is just given by Eq. (28), also out of equilibrium. In contrast, the impurity noise $S_{\rm imp}(x,x,\omega)$ is voltage dependent. Again we concentrate on the weak backscattering limit which amounts to performing a perturbative expansion in λ, up to order λ^2. In doing so the average value $\langle\ldots\rangle_\rightarrow$ can actually be replaced by the free average $\langle\ldots\rangle_0$. Thus, it can be shown that (up to order λ^2) the two contributions S_A and S_C to the impurity noise (23) read

$$S_A(x,x,\omega) = \frac{1}{4\pi}\left(\frac{h}{e^2}\right)^2 |\sigma_0(x,x_0,\omega)|^2 f_A^{(2)}(x_0,\omega)\,, \tag{47}$$

$$S_C(x,x,\omega) = -\frac{1}{\pi}\left(\frac{h}{e^2}\right)^2 \coth\left(\frac{\hbar\omega}{2k_BT}\right)\Re[\sigma_0(x,x_0,\omega)]\,\Re\left[\sigma_0(x,x_0,\omega)f_C^{(2)}(x_0,\omega)\right] \tag{48}$$

with

$$\begin{aligned} f_A^{(2)}(x_0,\omega) &= 4\pi\left(\frac{e\lambda}{\hbar}\right)^2\int_0^\infty dt\cos(\omega t)\cos(\omega_0 t)\sum_{s=\pm}e^{4\pi C_0(x_0,st;x_0,0)} \\ &= 4\pi\left(\frac{e\lambda}{\hbar}\right)^2\frac{i}{2}\sum_{q=\pm}\coth\left(\frac{\hbar(\omega+q\omega_0)}{k_BT}\right)\int_0^\infty dt\,\sin((\omega+q\omega_0)t)\sum_{s=\pm}se^{4\pi C_0(x_0,st;x_0,0)}\,, \end{aligned} \tag{49}$$

and

$$f_C^{(2)}(x_0,\omega) = 2\pi\left(\frac{e\lambda}{\hbar}\right)^2\int_0^\infty dt\,(e^{i\omega t}-1)\cos(\omega_0 t)\sum_{s=\pm}se^{4\pi C_0(x_0,st;x_0,0)}\,, \tag{50}$$

where $\omega_0 = eV/\hbar$, and

$$\sigma_0(x, x_0, \omega) = (1-\gamma)\frac{e^2}{h}\frac{e^{i\omega(\frac{x}{L}-\frac{1}{2})/g\omega_L}}{1-\gamma^2 e^{2i\omega/\omega_L}}\left(e^{i\frac{\omega}{\omega_L}(\frac{1}{2}-\xi_0)} + \gamma e^{i\frac{\omega}{\omega_L}(\frac{3}{2}+\xi_0)}\right) . \quad (51)$$

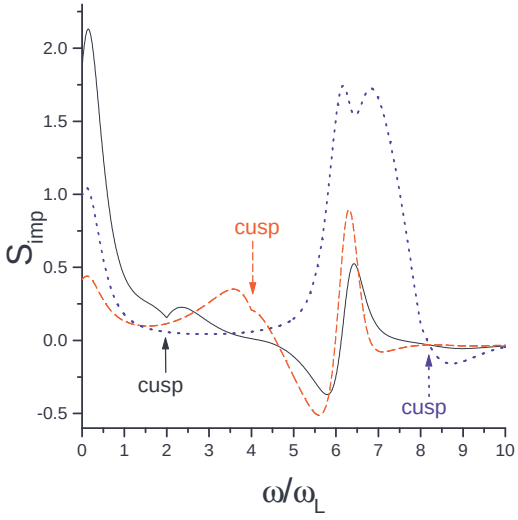

FIG. 12: The frequency spectrum of the non-equilibrium impurity noise $S_{\rm imp}$ (in units of $e^2\omega_L(\lambda^*/\hbar\omega_L)^{2(1-g)}$), at $T = 0$, for three different values of the dimensionless voltage $u = eV/\hbar\omega_L$: $u = 2$ (solid curve), $u = 4$ (dashed curve), and $u = 8$ (dotted curve). The interaction strength is $g = 0.25$ and the impurity position is $\xi_0 = 0$. $S_{\rm imp}$ has a cusp singularity at $\omega = eV/\hbar$.

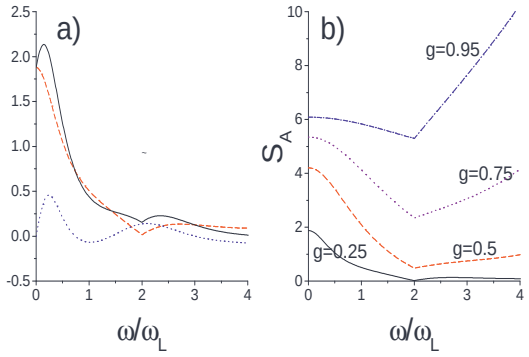

FIG. 13: a) The frequency spectra of the two contributions S_A (dashed curve) and S_C (dotted curve) to the impurity noise $S_{\rm imp} = S_A + S_C$ (solid curve) show that the presence of the cusp is due to S_A. The value of the dimensionless voltage is $u = 2$, and the other parameters are chosen as in Fig. 12. b) The contribution S_A for four different values of the interaction strength: $g = 0.25$ (solid curve), $g = 0.50$ (dashed curve), $g = 0.75$ (dotted curve), and $g = 0.95$ (dash-dotted curve). The interaction modifies the slope to the right and to the left of the singularity at $\omega = eV/\hbar$.

In Eq. (51), x is assumed to be in the right lead. Importantly, the modulus square of Eq. (51)

$$\left(\frac{h}{e^2}\right)^2 |\sigma_0(x, x_0, \omega)|^2 = (1-\gamma)^2\frac{1+\gamma^2+2\gamma\cos(2\omega(\xi_0+1/2)/\omega_L)}{1+\gamma^4-2\gamma^2\cos(2\omega/\omega_L)} \quad (52)$$

is independent of x, and thus $S_A(x, x, \omega)$ is independent of x. However, the r.h.s. of Eq. (47) depends on the position of the impurity x_0. With the help of Eq. (49) one sees that Eq. (47) has a form similar to Eq. (12), the backscattering current at the impurity.

We discuss now the non-equilibrium properties of the spectrum $S_{\rm imp}(x, x, \omega)$ of the impurity noise, considering for simplicity the case of a centered impurity at $\xi_0 = 0$. We first analyze the case of zero temperature, where a non-analyticity at the frequency $\omega_0 = eV/\hbar$ arises. In Fig. 12, one can see the discontinuity of the derivative of $S_{\rm imp}$ with respect to the frequency. This singularity stems from the contribution S_A to the impurity noise $S_{\rm imp}$, as shown in Fig. 13a. Thus, in regimes where S_A is dominated by S_C, the singularity is hardly visible: this is the case when the interaction is strong and when $\omega \sim \omega_0 \gg \omega_L$, as for the dotted curve in Fig. 12.

This non-analyticity of the noise at $\omega = \pm\omega_0$ is already present in a non-interacting wire where it arises from the sharpness of the Fermi surface at $T = 0$.[50] This is recovered in our model by taking the limit $g \to 1$. In this limit, S_A turns out to describe current fluctuations due to electrons originating from different reservoirs (the left and the right one), whereas S_C comes from current fluctuations due to electrons originating from the same reservoir (see e.g. Ref. [23]). When electron-electron interaction is taken into account ($g < 1$), the slope of the branches of S_A below and above the singularity is modified. While for a non-interacting system S_A is frequency-independent for $\omega \lesssim \omega_0$ and proportional to $\omega - \omega_0$ for $\omega \gtrsim \omega_0$, in the interacting case, one finds interaction dependent slopes, clearly shown in Fig. 13b. Thus, the type of singularity at $\omega = \pm\omega_0$ turns out to be essentially unchanged by the interaction, in particular, the location of the cusp is not modified. We emphasize that this prediction is different from the results for the homogeneous TLL, where the linear dependence $\propto |\omega \pm \omega_0|$ is turned into a g-dependent power-law $|\omega \pm \omega_0|^{2g-1}$.[24,48] Hence, this power-law is masked by the presence of the leads.

In the case of finite temperature, the cusp at $\omega = eV/\hbar$ is smeared like in a non-interacting wire, i.e. through a

$\coth[\hbar(\omega \pm \omega_0)/k_B T]$ prefactor (see Eq. (49)).

1. Shot noise regime

The ideal shot noise is defined as the value of the noise at zero temperature and zero frequency. In this limit, the ratio of the current noise and the backscattering current is related to the charge that is transferred in each backscattering event.[23] For the system under consideration, it has already been shown[26,27] that the shot noise is independent of x and can be written as

$$S(x,x,0) = 2eI_{\rm BS} \ , \tag{53}$$

where the backscattering current $I_{\rm BS}$ is given by Eq. (10). This result can be easily seen from the expressions for the current and noise at order λ^2 derived above. For $T = 0$ and $\omega = 0$ the terms in Eqs. (12) and (49) with '$s = -1$' vanish and $S_A(x,x,0)$ is the only contribution to the noise (S_0 and S_C vanish for $T = 0$ and $\omega = 0$). This is why $S(x,x,0)$ and $I_{\rm BS}$ are related to each other by the simple relation (53). Hence, if $\omega \ll \omega_L$, the fractional charge of the charge excitations that are backscattered at an impurity in a TLL[51,52] does not become visible through the Fano factor $F = S/2eI_{\rm BS}$. Instead, Eq. (53) just reveals the electron charge e.

Since this is a consequence of the fact that at very low frequencies one probes the charge dynamics at long length scales, larger than the wire length L, it should be interesting to look at frequencies near ω_L, where the current noise is expected to become sensitive to internal backscattering processes in the wire. In particular, it will be shown below that a voltage and temperature regime exists in which the frequency behavior of the noise is given by

$$S(x,x,\omega) \simeq 2eF(\omega)I_{\rm BS} \ . \tag{54}$$

Here the function $F(\omega)$, which plays the role of an effective Fano factor, reads

$$F(\omega) = \frac{h^2}{e^4} \left|\sigma_0(x,x_0,\omega)\right|^2 \ , \tag{55}$$

where $\sigma_0(x,x_0,\omega)$ is given by Eq. (52). Before discussing in detail the parameter regime in which the noise acquires the simple form (54), we want to comment on the physical contents of this relation.

As shown in Ref. [31], the effective Fano factor $F(\omega)$ allows to determine the fractional charge of the quasiparticles of the interacting wire. Importantly, Eq. (55) does not depend on temperature since the conductivity of the clean wire is temperature independent. An explicit expression for $F(\omega)$ is obtained by inserting Eq. (52) into Eq. (55). In doing so, one can realize that F is actually also independent of the point of measurement x, but it depends on the impurity position x_0.

We first describe the case of a centered impurity, i.e. $\xi_0 = x_0/L = 0$; in this case the Fano factor reads

$$F(\omega) = \frac{2g^2}{1+g^2-(1-g^2)\cos(\omega/\omega_L)} \ , \tag{56}$$

and its behavior as a function of ω is shown in Fig. 14. The choice of a centered impurity also allows us to compare the noise of the finite length wire with the noise obtained within the homogeneous TLL model. The latter model corresponds, in a sense, to the limit $L \to \infty$ of our model with a fixed impurity position x_0, hence, $\xi_0 = x_0/L \to 0$.

Let us discuss several limits of Eq. (54). Since $F(0) = 1$, in the limit $\omega \to 0$, Eq. (54) yields the interaction-independent result (53). Evidently, one has to go to finite frequency to obtain more interesting results. If we again adopt the averaging procedure (39), and note that the average value of $F(\omega)$ is the interaction parameter g (see Fig. 14), we obtain[53]

$$\langle S(x,x,\omega)\rangle_{\Delta\omega_1} \simeq 2egI_{BS} \, . \tag{57}$$

Seemingly, Eq. (57) suggests that quasiparticles with a fractional charge $e^* = eg$ are backscattered off the impurity in the TLL. For $L \to \infty$ the Fano factor (56) becomes a rapidly oscillating function, and the frequency interval $\Delta\omega_1$ over which $F(\omega)$ is averaged in Eq. (57) vanishes. This result should therefore describe the noise of the homogeneous TLL model with an impurity[28] as it is indeed the case. Hence, our findings are in accordance with previous considerations of the effects of an impurity in a TLL.[51,52]

We now discuss in detail the conditions under which the simple expression (54) holds. In particular, we consider the parameter regime $eV \gg \{k_B T, \hbar\omega, \hbar\omega_L\}$ (which will be referred henceforth as the *shot noise regime*). We write the noise as

$$S(x,x,\omega) = 2eF(\omega)\, I_{\rm BS}\, [\Delta_A + \Delta_C + \Delta_0] \tag{58}$$

with the functions $\Delta_\alpha = S_\alpha/2eF(\omega)I_{\rm BS}$, where the subscript α takes the values $\alpha = A, C, 0$, and the S_α are respectively given by Eqs. (28), (47), and (48). Using these formulas, one can then evaluate Δ_A, Δ_C, and Δ_0 in the shot noise regime. The range of validity of Eq. (54) corresponds to a parameter regime in which $\Delta_A \simeq 1$, $|\Delta_C|, |\Delta_0| \ll 1$. The main contribution to the shot noise thus stems from S_A.

Indeed, in the shot noise regime S_A can easily be shown to read

$$\begin{aligned} S_A(x,x,\omega) \ &= \ e\,F(\omega)\,[I_{\rm BS}(eV+\hbar\omega) + I_{\rm BS}(eV-\hbar\omega)] \\ &\times \ \left\{1 + \mathcal{O}\left[\exp\left(\frac{k_B T}{eV \pm \hbar\omega}\right)\right]\right\} \end{aligned} \tag{59}$$

which gives

$$\Delta_A \ \simeq \ \frac{I_{\rm BS}(eV+\hbar\omega) + I_{\rm BS}(eV-\hbar\omega)}{2I_{\rm BS}(eV)} \ , \tag{60}$$

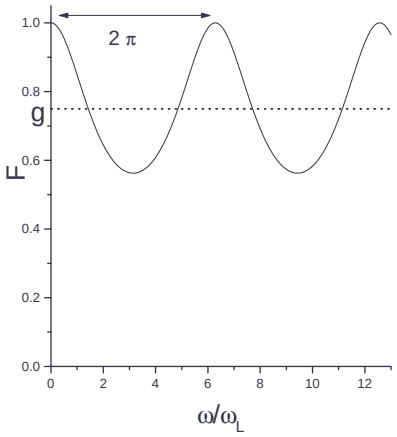

FIG. 14: The periodic function $F(\omega)$ defined in Eq. (56) is plotted for $g = 0.75$ against ω/ω_L. While $F(0) = 1$, the average over one period yields the interaction parameter g.

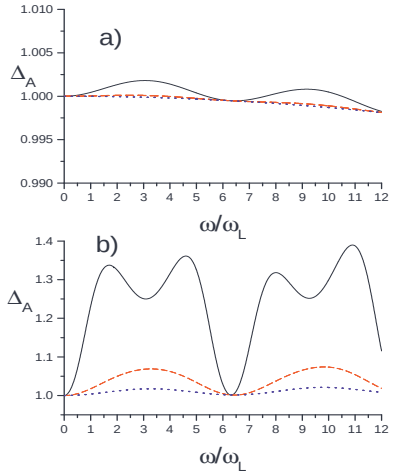

FIG. 15: The dimensionless quantity Δ_A defined in the text as a function of frequency in the shot noise regime $eV \gg \{k_BT, \hbar\omega, \hbar\omega_L\}$. The value of the dimensionless voltage is $u = eV/\hbar\omega_L = 100$, and the impurity is located in the middle $\xi_0 = 0$. Differences between the exact value of Δ_A and its approximation (60) are not visible. a) refers to the case of weak interaction $g = 0.75$ and b) to the case of strong interaction $g = 0.25$. The three different curves in each plot correspond to three different values of the dimensionless temperatures $\Theta = k_BT/\hbar\omega_L$, $\Theta = 0$ (solid), $\Theta = 1$ (dashed), and $\Theta = 2$ (dotted). Notice the different scales in the two cases: For weak interaction even small temperatures allow to fulfill the requirement $\Delta_A \simeq 1$, whereas for strong interaction a temperature of the order of $\Theta \simeq 2 - 3$ is required.

where the omitted terms are exponentially small corrections. Eq. (60) reveals that Δ_A can be directly extracted from the current voltage characteristics. As shown in Fig. 15 for the case of $eV = 100\hbar\omega_L$, in order to make the deviations from $\Delta_A = 1$ negligible, one has to operate at a sufficiently high temperature, so that the oscillations of the current are damped. For weak interactions ($g \simeq 0.75$) a temperature of the order of $k_BT \simeq \hbar\omega_L$ or even smaller is already sufficient to fulfill this requirement, whereas for strong interaction ($g \simeq 0.25$) higher temperatures of the order of $k_BT \simeq 2 - 3\hbar\omega_L$ are necessary.

We now turn to the correction Δ_C. In the low frequencies range ($\omega \lesssim \omega_L$), Δ_C can be written as

$$|\Delta_C| = \frac{2\hbar\omega}{eV} \coth\left(\frac{\hbar\omega}{2k_BT}\right) \left[|\kappa_{\rm BS}(V)| + \mathcal{O}\left(\frac{\omega}{\omega_L}\right)^2\right], \tag{61}$$

where the quantity $\kappa_{\rm BS}(V)$ is defined in Eq. (21). Here, one can again distinguish two cases. For weak interaction, $\kappa_{\rm BS}(V)$ is a slowly decreasing function of voltage, of the order of $2g - 1$ (see Fig. 5b). Therefore $|\Delta_C| \ll 1$ requires $eV \gg \max\{k_BT, \hbar\omega, \hbar\omega_L\}$. In contrast, for strong interaction $\kappa_{\rm BS}(V)$ exhibits large oscillations increasing with voltage (see Fig. 5a), which might yield very large values of Δ_C. To recover the simple behavior (54), it is therefore crucial to exploit these oscillations by choosing voltage values at which $\kappa_{\rm BS}(V) \approx 0$. Thus, with a suitable choice of temperature and voltage, the condition $|\Delta_C| \ll 1$ can always be fulfilled in the low frequency range. When this is the case, it turns out from the numerical analysis that the condition $|\Delta_C| \ll 1$ then remains valid up to frequencies $\omega \sim 10\,\omega_L$.

Finally, to obtain an estimate of Δ_0, we observe that the backscattering current can be written as $I_{\rm BS} = (e^2/h)\mathcal{R}V$, where $\mathcal{R} \ll 1$ is an effective reflection coefficient that can be directly extracted from a current-voltage measurement. In contrast to a non-interacting wire, $\mathcal{R}$ now depends in general on voltage, interaction strength, and temperature. Since the (temperature independent) function $(h/e^2)\Re[\sigma_0(x, x, \omega)]/F(\omega)$ has a maximum $\mathcal{C}$, we obtain for Δ_0 the upper bound

$$|\Delta_0| \leq \coth\left(\frac{\hbar\omega}{2k_BT}\right) \frac{\hbar\omega}{eV\mathcal{R}}\mathcal{C}\,. \tag{62}$$

The value of $\mathcal{C}$ depends on the interaction strength. For relatively weak interaction ($g \simeq 0.75$) one has $\mathcal{C} \simeq 1$, whereas for strong interaction ($g \simeq 0.25$) $\mathcal{C} \simeq 4$. Thus, the condition $|\Delta_0| \ll 1$ is certainly fulfilled in the parameter range $eV\mathcal{R} \gg \mathcal{C}\max\{k_BT, \hbar\omega, \hbar\omega_L\}$.

In summarizing these considerations, we see that a noise measurement in the parameter regime $eV\mathcal{R} \gg \mathcal{C}\hbar\omega$ allows to extract the Fano factor $F(\omega)$ from noise data. The optimal temperature at which one should operate depends on the QW under investigation. In particular, for systems characterized by weak or moderate interaction ($g \simeq 0.75$), like for most semiconductor QWs, the optimal temperature is $k_BT/\hbar\omega_L \lesssim 1$, while for strong interaction ($g \simeq 0.25$), like for SWNTs, a temperature $k_BT/\hbar\omega_L \simeq 2 - 3$ is more appropriate. On the other hand, the voltage needs to be rather high to fulfill in particular the condition $\Delta_0 \ll 1$. However, this prob-

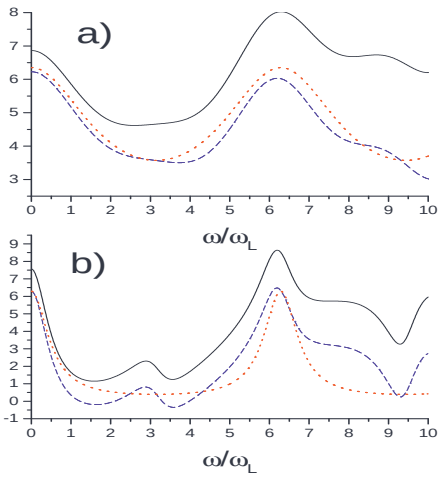

FIG. 16: The frequency spectrum of the full noise $S(x,x,\omega)$ (solid line) in units of $e^2\omega_L$ and the approximation (54) (dotted line) are depicted for two systems with the parameters a) $g=0.75$, $\Theta=1$, $u=100$, $\delta_x=0.05$, $\xi_0=0$, $\mathcal{R}=0.2$ and b) $g=0.25$, $\Theta=2$, $u=98.83$, $\delta_x=0.05$, $\xi_0=0$, $\mathcal{R}=0.2$. The dashed curve is obtained after a background subtraction (see text).

lem can be at least partially overcome by an appropriate background subtraction. This is demonstrated in Fig. 16 for the cases of weak and strong interaction, respectively.

Fig. 16a refers to a weakly interacting QW with interaction parameter $g=0.75$. The temperature $k_BT=\hbar\omega_L$ and the voltage $eV=100\hbar\omega_L$. The impurity is assumed to be in the middle, i.e., $\xi_0=0$, and the measurement point is near a contact so that $\delta_x=0.05$. The impurity leads to an effective reflection coefficient $\mathcal{R}=0.2$ which correspond to an effective impurity strength $\lambda^*\sim 10^{-4}eV$. For these parameters the full noise has still a sizable contribution from S_0, as can be estimated from Eq. (62), which gives for frequencies $\omega\sim\pi\omega_L$ and the above parameters $\Delta_0\sim 0.2$. A simplified estimate for S_0 reads

$$S_{\rm off-set}=\frac{e^2}{\pi}\omega\coth(\hbar\omega/2k_BT)\,, \qquad (63)$$

which can be subtracted from the full noise to give the dashed curve in Fig. 16a. When this curve is averaged between $\omega=0$ and the first maximum, one extracts $g\sim 0.71$, which is a reasonable estimate of 0.75.

Fig. 16b refers to a strongly interacting QW with interaction parameter $g=0.25$. Here, the temperature $k_BT=2\hbar\omega_L$ and the voltage $eV=98.83\hbar\omega_L$, a value chosen with the help of the current voltage characteristic in such a way that $\kappa_{\rm BS}=0$. This makes the contribution of S_C negligible, as discussed above, cf. Eq. (61). The impurity is again assumed to be in the middle, i.e., $\xi_0=0$, and the measurement point corresponds to $\delta_x=0.05$. The effective reflection coefficient $\mathcal{R}=0.2$ now comes from an impurity with effective strength $\lambda^*\sim 0.12eV$. For these parameters the full noise has a large contribution from S_0, since Eq. (62) gives $\Delta_0\sim 0.6$ for frequencies $\omega\sim\pi\omega_L$. Despite this large value of Δ_0, the value of g can still be extracted. A subtraction of $S_{\rm off-set}$ leads to the dashed curve in Fig. 16b. When this curve is averaged between $\omega=0$ and the second maximum, where the noise reaches again the same level as at low frequencies, one obtains $g\sim 0.23$, again a reasonable estimate of 0.25. A more accurate data analysis can, of course, be based on the full expressions for the noise derived above.

We mention that a similar procedure can be provided for the case of an off-centered impurity. For an arbitrary impurity position x_0, the Fano factor reads

$$F(\omega)=(1-\gamma)^2\frac{1+\gamma^2+2\gamma\cos\left(\frac{2\omega(\xi_0+1/2)}{\omega_L}\right)}{1+\gamma^4-2\gamma^2\cos\left(\frac{2\omega}{\omega_L}\right)}\,, \qquad (64)$$

where again $\xi_0=x_0/L$. When compared to the case of a centered impurity, we observe that now for certain noise frequencies a pronounced reduction of the Fano factor occurs, as discussed in Ref. [31]. This effect could be related to the low Fano factor measured in bundles of carbon nanotubes.[35] Secondly, since Eq. (64) is not in general a periodic function, the averaging procedure used in Eq. (57) to derive g cannot be applied. However, one can always introduce the function

$$Fi(\Omega)=\frac{1}{\Omega}\int_0^\Omega F(\omega)\,d\omega\,, \qquad (65)$$

which is a generalization of the averaging defined in Eq. (39). Interestingly, $Fi(\Omega)$ exhibits oscillations around the value g for any position ξ_0 of the impurity; these oscillations are damped with increasing Ω, and the value of g can be extracted, or at least relatively well estimated.

Despite the progress made recently with the measurement of high frequency noise,[33,54] it might be difficult to obtain accurate noise data up to frequencies of order $10\omega_L$, if the QW is not very long. Then, a more detailed analysis of low frequency noise data may be of particular interest. As we have shown previously[31], the interaction constant g could also be deduced from the low-frequency behavior of the Fano factor (64)

$$F(\omega)=1-\left(\frac{\omega L}{2v_F}\right)^2(1-g^2)\left[1+4g^2\xi_0(1+\xi_0)\right]+\mathcal{O}\left(\frac{\omega}{\omega_L}\right)^4$$

once the position of the impurity is known. The latter can be determined from the current voltage characteristics by tuning the temperature, as described in Sec. III.

We conclude this discussion of the shot noise by mentioning another interesting feature emerging in this regime, namely the fact that the slope of the noise at

$\omega = 0$ is related to the differential conductance. Explicitly, we obtain

$$\lim_{\omega\to 0} \frac{S(x,x,\omega) - S(x,x,0)}{2\hbar\omega(e^2/h)} = \left(\frac{h}{e^2}\frac{dI}{dV}\right)^2 . \qquad (66)$$

This result has been derived perturbatively in the impurity strength including terms up to order λ^2 and is in agreement with the Coulomb gas calculation for the homogeneous TLL model.[48] Moreover, in the limit $g \to 1$, Eq. (66) coincides with the corresponding expression for non-interacting electrons.[23] We note that the limits $V \to 0$ and $\omega \to 0$ are not interchangeable, since from Eq. (41) the slope of the noise at equilibrium ($V = 0$) is proportional to the linear conductance, and not to its square. The simple relation Eq. (66) between the slope of the noise and the dimensionless differential conductance is only valid at zero temperature; in addition, an exact solution of the homogeneous TLL model[49] indicates that such a simple relation may not hold if all orders in the impurity strength are taken into account in a non-perturbative way.

C. Excess noise

In the previous subsections we have discussed the equilibrium noise and the non-equilibrium noise. In the present section we focus on the excess noise, which is simply defined as their difference

$$S_E(x,x,\omega) = S(x,x,\omega) - S(x,x,\omega)|_{V=0} . \qquad (67)$$

Since the S_0 contribution to the noise does not depend on the voltage, S_E is independent of S_0 and therefore a quantity arising entirely from the presence of the impurity. For this reason, the excess noise is of particular interest. The impurity strength appears in S_E as an overall scaling factor. In contrast, in the full noise the presence of S_0, which is independent of the impurity strength, requires a background subtraction to reveal the interesting effects related to impurity backscattering. We notice that S_E can also be written as

$$S_E(x,x,\omega) = S_{\rm imp}(x,x,\omega) - S_{\rm imp}(x,x,\omega)|_{V=0} \qquad (68)$$

with

$$S_{\rm imp}(x,x,\omega)|_{V=0} = 2\hbar\omega \coth\left(\frac{\hbar\omega}{2k_BT}\right) \Re[\sigma_{\rm BS}(x,x,\omega)],$$

where $\sigma_{\rm BS}(x,y,\omega)$ is given in Eq. (46).

The behavior of the excess noise is illustrated in Fig. 17. We first focus on Fig. 17a, which refers to the case of strong electron interaction ($g = 0.25$). Then, apart from some special points along the diagonal, the structure of the excess noise essentially exhibits a voltage independent behavior, as the horizontally oriented shape suggests. Indeed, for strong interaction and for moderate to high frequencies ($\omega \gtrsim \omega_L$), the excess noise is dominated by the equilibrium noise, in particular, by the supplementary noise $S_{\rm imp}$ at equilibrium, i.e., $S_E \simeq -S_{\rm imp}|_{V=0}$. Deviations from this behavior lead to the spots along the diagonal of the excess noise diagram. These spots appear whenever $eV/\hbar$ equals a frequency corresponding to a peak of the equilibrium noise. Then, the excess noise acquires a non negligible contribution also from the finite voltage term, and the simple formula $S_E \simeq -S_{\rm imp}|_{V=0}$ is not valid. As discussed in Sec. IV A 2, these particular frequency values are determined by $\Im[\sigma_0^2(x,x_0,\omega)]$.

Let us now consider the case of weaker interaction strength. The evolution of the excess noise in Fig. 17 from a) to d) shows that the scenario dramatically changes, even at the qualitative level: The horizontal lines smear out and a diagonally oriented shape arises. A very sharp diagonal structure is precisely the expected behavior of the excess noise in the noninteracting limit, where S_E is given by[23]

$$S_E = \frac{e^2}{h}\begin{cases} 0 & \hbar|\omega| > eV \\ 2(eV - \hbar|\omega|)\mathcal{R}(1-\mathcal{R}) & \hbar|\omega| < eV, \end{cases} \qquad (69)$$

where $\mathcal{R}$ is the reflection coefficient. Still, some qualitative differences compared to the noninteracting case are present. While for the non-interacting system the excess noise is always strictly non-negative, regions of negative excess noise emerge for the interacting case. The fact that the excess noise S_E can be *negative* may be surprising, since the presence of an applied voltage is expected to increase the noise. However, we deal here with a non-linear system, where the voltage also affects the interference conditions between plasmonic charge excitations that are Andreev-type reflected at the contacts and backscattered by the impurity. Thus, depending on V, the interference can be destructive or constructive, and – under certain circumstances – the equilibrium noise can be larger than the corresponding non-equilibrium noise at the same noise frequency ω.

V. CONCLUSIONS

In the present work, we have investigated transport properties of interacting quantum wires with a weak impurity coupled to non-interacting (Fermi liquid) electron reservoirs. We have used the inhomogeneous Tomonaga Luttinger liquid model with a backscattering term to describe the system, and the Keldysh formalism to predict its transport properties out of equilibrium. It has been shown that the finite length L of the quantum wire crucially affects the transport properties.

On the one hand, the nonlinear $I - V$ characteristics becomes an oscillating function of the applied voltage, an effect which is washed out if the temperature is raised. It has also been shown that, with an appropriate choice of the temperature, these oscillations can be exploited

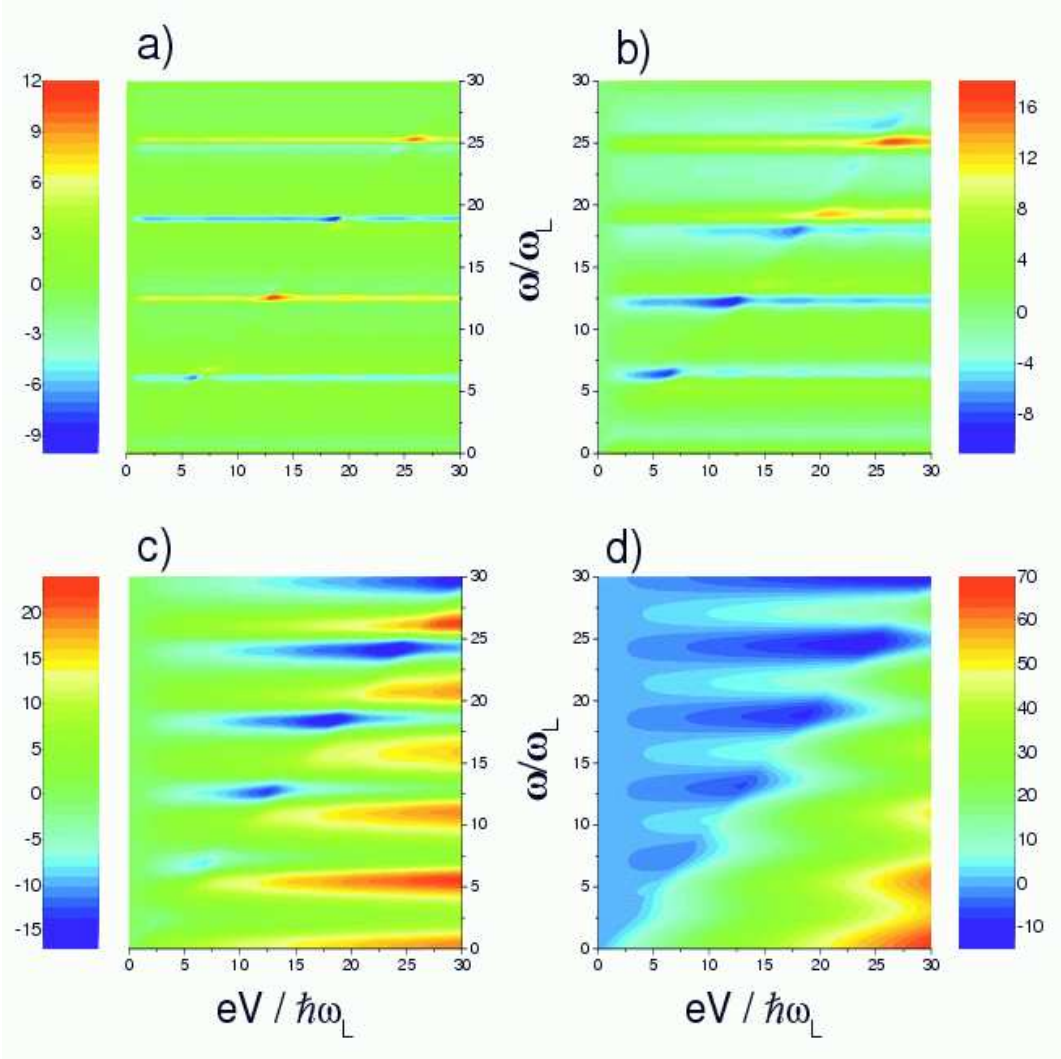

FIG. 17: The excess noise at zero temperature and for an impurity in the middle of the wire ($\xi_0 = 0$) is shown (in units of $e^2\omega_L(\lambda^*/\hbar\omega_L)^{2(1-g)}$) as a function of the dimensionless frequency ω/ω_L and the applied voltage $eV/\hbar\omega_L$ for four values of interaction strength: a) $g = 0.25$; b) $g = 0.5$; c) $g = 0.75$; d) $g = 0.95$.

to measure both the interaction strength g and the position of an impurity in the wire. We wish to emphasize that these oscillations are not due to nonadiabatic contacts, which would lead to ordinary Fabry-Pérot oscillations that are also present in a noninteracting wire. Instead, the oscillations predicted here arise because of a mismatch of the strength of the electron-electron interaction in the quantum wire and the leads. Therefore, a measurement of these current oscillations would provide evidence for electronic correlations in one-dimensional systems. From the above remarks it is clear that one needs a way to distinguish experimentally the current oscillations due to a mismatch of the electron-electron interaction from ordinary Fabry-Pérot oscillations. We propose to vary the voltage of a metallic back-gate that influences the electron density in the quantum wire, since the ordinary Fabry-Pérot oscillations are highly affected by a change of the gate voltage.[40,55] In contrast, this is not necessarily the case for the oscillations predicted here. More precisely, if the distance between the one-dimensional channel and the gate electrode does not depend on the gate voltage, the interaction parameter g is essentially independent of the applied gate voltage, and the oscillations predicted here should not be affected much by a change of the gate voltage. This will typically be the case for a SWNT on an oxidized substrate. In semiconductor QWs a weak dependence of g on the gate voltage has to be expected. However, the gate voltage dependence seems to be a decisive factor distinguishing Fabry-Pérot oscillations from the oscillations predicted by us.

On the other hand, we have shown that, similarly to the average current, also the frequency spectrum of the current noise significantly depends on the interaction

strength and the finite length of the wire. At frequencies $\omega \ll \omega_L = v_F/gL$, the noise is determined by slow processes, much slower than the traversal time of a plasmon through the interacting wire, and the noise is not affected by the presence of electron-electron interaction. This is similar to the absence of a suppression of the DC conductance by the interaction in a one-dimensional quantum wire connected to Fermi liquid leads. In the limit $\omega \to 0$, internal properties of the interacting wire cannot be resolved, and the wire with the impurity effectively behaves as a complicated scatterer between two Fermi liquid leads. However, for noise frequencies of the order of ω_L, the situation changes both for the equilibrium and the non-equilibrium case.

In particular the equilibrium noise, related to the AC conductivity by the FDT, has been shown to exhibit oscillations as a function of ω already in the absence of impurities in the wire. These oscillations are characterized by two frequencies, where the larger one is proportional to the ballistic frequency related to the length of the wire, while the smaller one depends on the distance of the measurement point of the noise from the nearby contact. An average over the fast oscillations allows to obtain a sinusoidal spectrum whose amplitude is directly connected to the interaction strength. In the presence of an impurity there is a supplementary equilibrium noise $S_{\rm imp}$. For a strongly interacting QW, $S_{\rm imp}$ is characterized by sharp spikes due to resonance phenomena caused by the Andreev-type reflections at the contacts and the backscattering at the impurity.

In presence of an applied voltage, we have seen that the zero temperature noise spectrum has cusps at the frequencies $\omega = \pm eV/\hbar$, as it is already the case for a noninteracting wire. We have shown that the electronic correlations affect the value of the slopes on both sides of these singularities in a different way. In contrast to predictions based on the homogeneous TLL model, the type of singularity is however not changed.

We have then focussed on the shot noise regime ($eV \gg \{k_BT, \hbar\omega, \hbar\omega_L\}$), where the system is strongly out of equilibrium. In this case, the scattering processes at the impurity are known to obey Poissonian statistics, and the noise is proportional to the backscattering current. The value of the Fano factor (ratio between S and $I_{\rm BS}$) strongly depends on the frequency range one explores. If ω is of the order of the ballistic frequency ω_L or larger, the Fano factor depends on g. This dependence becomes particularly simple if the impurity is located in the middle of the wire. In that case, $e^* = eg$ appears as a prefactor of the finite frequency noise, when it is averaged over an appropriate frequency range. This may allow for an independent way to measure g. The most promising range of parameters for such an experiment as well as possible improvements of the data analysis by a background subtractions have been thoroughly discussed. Moreover, it has been shown that relevant information is already contained in the low frequency noise data.

We also mention that in realistic one-dimensional systems, like SWNTs or cleaved edge overgrowth QWs, typical values of the Fermi velocity are $v_F \sim 10^5 \div 10^6$m/s. The length of the wires can vary from 1μm up to tenths of μm, whereas the typical interaction strengths are $g \sim 0.2$ for SWNTs and $g \sim 0.7$ for semiconductor QWs. These values yield estimates of the ballistic frequency $\hbar\omega_L$ of order meV or below.[56,57] The conditions $eV \gg \hbar\omega_L$ and $\omega \gg \omega_L$ for the observability of the current oscillations and the fractional charge are therefore experimentally realistic according to nowadays techniques.[33,34] Moreover, the constraints for experiments in the shot noise regime could be significantly relaxed, provided that the experimental setup enables a measurement of the supplementary noise $S_{\rm imp} = S_A + S_C$ instead of the full noise S only. Then, the condition $\Delta_0 \ll 1$ is redundant, and one is left with the weaker conditions $\Delta_A \simeq 1$ and $\Delta_C \ll 1$, which amount to require $eV \gg \hbar\omega$, and $k_BT/\hbar\omega_L \lesssim 1$ ($k_BT/\hbar\omega_L \sim 2-3$) for weak (strong) interaction. Such experiments could be based on a quantum wire with a tunable impurity, which could, for instance, be realized by two crossed carbon nanotubes[58] or a nanotube with a nearby STM tip.

Acknowledgments

Helpful discussions with H. Bouchiat, R. Deblock, R. Egger, D. C. Glattli, K.-V. Pham, F. Piechon, P. Roche, and H. Saleur are gratefully acknowledged. Financial support was provided by the EU networks DIENOW and SPINTRONICS.

APPENDIX A: KELDYSH PATH-INTEGRAL FORMULATION

In this appendix, we provide details of the method to calculate transport properties of the system by adopting the Keldysh formalism.[59]

In the Hamiltonian (1), the term (4) can equivalently be replaced by

$$\mathcal{H}'_V = \frac{1}{\sqrt{\pi}} \int_{-\infty}^{+\infty} \partial_x \mu(x)\, \Phi(x,t) dx\,. \qquad \text{(A1)}$$

Both forms yield the same equations of motion; however, the latter form is more suitable for the manipulations to be presented below.

In the case of a constant applied voltage we have from Eq. (5)

$$\partial_x \mu = -\mu_L \delta(x + \frac{L}{2}) + \mu_R \delta(x - \frac{L}{2}), \qquad \text{(A2)}$$

but much of the following derivation is actually valid for any function, including also time-dependent ones. For

this reason, instead of (A1), we shall consider here a general term of the form

$$\mathcal{H}'_V = -\frac{e}{\sqrt{\pi}} \int_{-\infty}^{+\infty} E(x,t)\, \Phi(x,t) dx\,. \qquad \text{(A3)}$$

The reader will be alerted whenever the quantity $-eE(x,t)$ will explicitly be replaced by the expression (A2).

Let us now denote by Φ^+ and Φ^- the complex fields on the upper and lower time branch of the Keldysh contour and introduce the generating functional

$$\begin{aligned} Z[J] &= \frac{1}{\mathcal{N}_{\mathcal{Z}}} \int \mathcal{D}\Phi^{\pm} \exp\left\{ -\frac{1}{2} \int d\mathbf{r}' d\mathbf{r}'' \sum_{\eta,\eta'=\pm} \Phi^{\eta}(\mathbf{r}') (\mathcal{C}_0^{-1})^{\eta,\eta'}(\mathbf{r}',\mathbf{r}'') \Phi^{\eta'}(\mathbf{r}'') \right\} \\ &\times \exp\left\{ \sum_{\eta=\pm} \left(-\frac{i}{\hbar} \eta \int_{-\infty}^{+\infty} dt' \mathcal{H}_B[\Phi^{\eta}] + \frac{ie}{\hbar\sqrt{\pi}} \eta \int d\mathbf{r}' E(\mathbf{r}') \Phi^{\eta}(\mathbf{r}') + \frac{i}{\sqrt{2}} \int d\mathbf{x} J(\mathbf{x}) \Phi^{\eta}(\mathbf{x}) \right) \right\}, \qquad \text{(A4)} \end{aligned}$$

where the vector label $\mathbf{r}'$ stands for $\mathbf{r}' = (x', t')$, $\int d\mathbf{r}' = \int_{-\infty}^{+\infty} dt' \int_{-\infty}^{+\infty} dx'$, and $\mathcal{N}_{\mathcal{Z}}$ is a normalization factor, which assures that $Z[0] = 1$. In Eq. (A4), $\mathcal{C}_0^{-1}(\mathbf{r}', \mathbf{r}'')$ is the inverse of a 2×2 matrix defined by the four free correlators

$$\mathcal{C}_0^{\eta,\eta'}(\mathbf{r}';\mathbf{r}'') = \langle \Phi^{\eta}(\mathbf{r}') \Phi^{\eta'}(\mathbf{r}'') \rangle_0\,, \qquad \text{(A5)}$$

where $\langle \ldots \rangle_0$ indicates the average performed with respect to the free Hamiltonian (2) along the Keldysh contour.

For a wire with an impurity and in presence of an applied voltage, we have

$$\langle \Phi(\mathbf{x}) \rangle = \frac{1}{2} \sum_{\eta=\pm} \langle \Phi^{\eta}(\mathbf{x}) \rangle = \frac{-i}{\sqrt{2}} \left. \frac{\delta Z[J]}{\delta J(\mathbf{x})} \right|_{J=0}\,. \qquad \text{(A6)}$$

One can simplify the notation by introducing infinite-dimensional vectors and matrices where *both* $\mathbf{r}$ and η are component labels. Defining

$$\mathbf{\Phi} = \begin{pmatrix} \Phi^+(\mathbf{r}) \\ \Phi^-(\mathbf{r}) \end{pmatrix}, \qquad \text{(A7)}$$

$$\mathbf{J} = \begin{pmatrix} \frac{e}{\hbar}\sqrt{\frac{2}{\pi}} E(\mathbf{r}) \\ J(\mathbf{r}) \end{pmatrix}, \qquad \text{(A8)}$$

$$\mathsf{Q} = \frac{1}{\sqrt{2}} \begin{pmatrix} 1 & -1 \\ 1 & 1 \end{pmatrix} \delta(\mathbf{r} - \mathbf{r}'), \qquad \text{(A9)}$$

and

$$\mathsf{C}_0 = \begin{pmatrix} \mathcal{C}_0^{++}(\mathbf{r},\mathbf{r}') & \mathcal{C}_0^{+-}(\mathbf{r},\mathbf{r}') \\ \mathcal{C}_0^{-+}(\mathbf{r},\mathbf{r}') & \mathcal{C}_0^{--}(\mathbf{r},\mathbf{r}') \end{pmatrix}, \qquad \text{(A10)}$$

one can rewrite the generating functional (A4) as

$$\begin{aligned} Z[J] &= \frac{1}{\mathcal{N}_{\mathcal{Z}}} \int \mathcal{D}\mathbf{\Phi}\, e^{-\frac{1}{2}\left(\mathbf{\Phi}^T \mathsf{C}_0^{-1} \mathbf{\Phi} - 2i \mathbf{J}^T \mathsf{Q} \mathbf{\Phi}\right)} \qquad \text{(A11)} \\ &\times \exp\left\{ -\frac{i}{\hbar} \sum_{\eta=\pm} \eta \int_{-\infty}^{+\infty} dt' \mathcal{H}_B[\Phi^{\eta}] \right\}, \end{aligned}$$

where the superscript ^{T} indicates the transpose. Shifting the fields

$$\mathbf{\Phi} \to \mathbf{\Phi} + \mathbf{A}_J\,, \qquad \mathbf{A}_J = i \mathsf{C_0} \mathsf{Q}^T \mathbf{J}\,, \qquad \text{(A12)}$$

the generating functional can be factorized into

$$Z[J] = Z_0[J] Z_B[J]\,, \qquad \text{(A13)}$$

where Z_0 and Z_B are given below. In particular, Z_0 is the generating functional in the absence of a backscatterer and reads

$$Z_0[J] = e^{-\frac{1}{2}\mathbf{J}^T \tilde{\mathsf{C}}_0 \mathbf{J}} \qquad \text{(A14)}$$

with

$$\tilde{\mathsf{C}}_0 = \mathsf{Q} \mathsf{C}_0 \mathsf{Q}^T = \begin{pmatrix} 0 & \mathcal{C}_0^A(\mathbf{r};\mathbf{r}') \\ \mathcal{C}_0^R(\mathbf{r};\mathbf{r}') & \mathcal{C}_0^K(\mathbf{r};\mathbf{r}') \end{pmatrix}\,, \qquad \text{(A15)}$$

where

$$\begin{aligned} \mathcal{C}_0^A(\mathbf{r};\mathbf{r}') &= -\theta(t'-t) \langle [\Phi(\mathbf{r}), \Phi(\mathbf{r}')] \rangle_0\,, \qquad \text{(A16)} \\ \mathcal{C}_0^R(\mathbf{r};\mathbf{r}') &= \theta(t-t') \langle [\Phi(\mathbf{r}), \Phi(\mathbf{r}')] \rangle_0\,, \qquad \text{(A17)} \\ \mathcal{C}_0^K(\mathbf{r};\mathbf{r}') &= \langle \{\Phi(\mathbf{r}), \Phi(\mathbf{r}')\} \rangle_0\,. \qquad \text{(A18)} \end{aligned}$$

Exploiting the fact that $\mathcal{C}_0^A(\mathbf{r}';\mathbf{r}'') = \mathcal{C}_0^R(\mathbf{r}'';\mathbf{r}')$, we can rewrite Eq. (A14) as

$$Z_0[J] = \exp\left\{-\frac{1}{2}\int d\mathbf{r}'d\mathbf{r}'' J(\mathbf{r}')\mathcal{C}_0^K(\mathbf{r}';\mathbf{r}'')J(\mathbf{r}'') - \frac{e}{\hbar}\sqrt{\frac{2}{\pi}}\int d\mathbf{r}'d\mathbf{r}'' J(\mathbf{r}')\mathcal{C}_0^R(\mathbf{r}';\mathbf{r}'')E(\mathbf{r}'')\right\}. \tag{A19}$$

The second factor Z_B in (A13) is the generating functional

$$Z_B[J(\mathbf{r})] = \left\langle \exp\left(-\frac{i}{\hbar}\sum_{\eta=\pm}\eta\int_{-\infty}^{+\infty}\mathcal{H}_B[\Phi^\eta + A_J^\eta]\,dt'\right)\right\rangle_0, \tag{A20}$$

which weights the backscattering term, and where the dependence on the source field $J(\mathbf{x})$ is contained in the shift $\mathbf{A}_J$ defined in Eq. (A12). In components, the latter reads explicitly

$$A_J^\eta(\mathbf{r}) = A_0(\mathbf{r}) + \int \frac{d\mathbf{x}}{\sqrt{2}}\left[i\mathcal{C}_0^K(\mathbf{r};\mathbf{x}) + \eta\, i\mathcal{C}_0^A(\mathbf{r};\mathbf{x})\right]J(\mathbf{x}), \tag{A21}$$

where

$$A_0(\mathbf{r}) = \frac{e}{\sqrt{\pi}\hbar}\int d\mathbf{x}\, i\mathcal{C}_0^R(\mathbf{r};\mathbf{x})E(\mathbf{x}). \tag{A22}$$

Notice that A_0 is independent of η.

Using Eq. (A13), Eq. (A6) can be rewritten as

$$\langle\Phi(\mathbf{x})\rangle = \frac{-i}{\sqrt{2}}\left(\frac{\delta Z_0}{\delta J(\mathbf{x})} + \frac{\delta Z_B}{\delta J(\mathbf{x})}\right)\Big|_{J=0}. \tag{A23}$$

It is now useful to define a quantity which has the dimension of a current

$$j_B^\eta(\mathbf{r}) = -\frac{e}{\hbar}\frac{\delta\mathcal{H}_B}{\delta\Phi(\mathbf{r})}[\Phi^\eta + A_0^\eta]. \tag{A24}$$

Inserting Eqs. (A19) and (A20) into Eq. (A23), and exploiting the property

$$\frac{\delta A_J^\eta(\mathbf{r})}{\delta J(\mathbf{x})} = \frac{i\left(\mathcal{C}_0^K + \eta\mathcal{C}_0^A\right)(\mathbf{r};\mathbf{x})}{\sqrt{2}} = \frac{i\left(\mathcal{C}_0^K + \eta\mathcal{C}_0^R\right)(\mathbf{x};\mathbf{r})}{\sqrt{2}},$$

we find

$$\langle\Phi(\mathbf{x})\rangle = \frac{e}{\sqrt{\pi}\hbar}\int d\mathbf{r}'\, i\mathcal{C}_0^R(\mathbf{x};\mathbf{r}')E(\mathbf{r}') + \frac{1}{2e}\sum_{\eta=\pm}\int_{-\infty}^{+\infty}dt'\left(\eta\, i\mathcal{C}_0^K + i\mathcal{C}_0^A\right)(\mathbf{r}_\mathbf{0}';\mathbf{x})\left\langle j_B^\eta(\mathbf{r}_\mathbf{0}')\right\rangle_\rightarrow, \tag{A25}$$

where $\mathbf{r}_\mathbf{0}' = (x_0, t')$, $\mathbf{x} = (x,t)$, and $\langle\ldots\rangle_\rightarrow$ denotes an average along the Keldysh contour with respect to the shifted Hamiltonian

$$\mathcal{H}_\rightarrow = \mathcal{H}_0[\Phi] + \mathcal{H}_B[\Phi + A_0]. \tag{A26}$$

In the latter equation, $\mathcal{H}_0$ and $\mathcal{H}_B$ are given in Eqs. (2) and (3), and the field in $\mathcal{H}_B$ is shifted by A_0.

The current is now obtained from Eq. (7). Differentiating Eq. (A25) with respect to time and defining

$$\sigma_0(\mathbf{x};\mathbf{y}) = \frac{e^2}{h}2i\,\partial_t\mathcal{C}_0^R(\mathbf{x};\mathbf{y}), \tag{A27}$$

one obtains

$$\langle j(\mathbf{x})\rangle = I_0(\mathbf{x}) - I_{\rm BS}(\mathbf{x}) \tag{A28}$$

with

$$I_0(\mathbf{x}) = \int d\mathbf{r}'\sigma_0(\mathbf{x};\mathbf{r}')E(\mathbf{r}'), \tag{A29}$$

and

$$I_{\rm BS}(\mathbf{x}) = -\frac{\hbar\sqrt{\pi}}{e^2}\int_{-\infty}^{+\infty}dt'\sigma_0(\mathbf{x};\mathbf{r}_0')\left\langle j_B^+(\mathbf{r}_0')\right\rangle_\rightarrow. \tag{A30}$$

If we now specify to the particular form (A2), one can easily show that Eq. (A22) becomes

$$A_0(x,t) = A_0(t) = \frac{\omega_0 t}{2\sqrt{\pi}}, \tag{A31}$$

where $\omega_0 = eV/\hbar$ is the frequency related to the applied voltage V (see Eq. (6)). In this case, Eq. (A29) gives $I_0(\mathbf{x}) = e^2V/h$ and Eq. (A30) becomes

$$I_{\rm BS}(\mathbf{x}) = -\frac{2\pi\lambda}{e}\int_{-\infty}^{+\infty}dt'\,\sigma_0(\mathbf{x};\mathbf{r}_\mathbf{0}')\left\langle\sin\left[\sqrt{4\pi}\Phi^+(\mathbf{r}_\mathbf{0}') + 2k_Fx_0 + \omega_0t'\right]\right\rangle_\rightarrow. \tag{A32}$$

From an expansion of Eq. (A32) in terms of λ, we obtain for the average value of the backscattering current to leading

order in λ

$$\begin{aligned} I_{\rm BS}(\mathbf{x}) &= \frac{\pi\lambda^2}{2e\hbar}\int_{-\infty}^{+\infty} dt'\,\sigma_0(\mathbf{x};\mathbf{r}'_{\mathbf{0}})\int_{-\infty}^{+\infty} dt''\sum_{m,m',n=\pm} mm'n\,e^{i(m+n)2k_Fx_0}e^{i\omega_0(mt''+nt')} \\ &\qquad\times\left\langle e^{im\sqrt{\pi}(\Phi^+(\mathbf{r}''_{\mathbf{0}})+\Phi^-(\mathbf{r}''_{\mathbf{0}}))+im'\sqrt{\pi}(\Phi^+(\mathbf{r}''_{\mathbf{0}})-\Phi^-(\mathbf{r}''_{\mathbf{0}}))+in\sqrt{4\pi}\Phi^+(\mathbf{r}'_{\mathbf{0}})}\right\rangle_0 \\ &= \frac{\pi\lambda^2}{2e\hbar}\int_{-\infty}^{+\infty} dt'\,\sigma_0(\mathbf{x};\mathbf{r}'_{\mathbf{0}})\int_{-\infty}^{\infty} dt''\sum_{m=\pm} me^{im\omega_0(t''-t')}e^{4\pi\langle\Phi(\mathbf{r}''_{\mathbf{0}})\Phi(\mathbf{r}'_{\mathbf{0}})-\Phi^2(\mathbf{r}'_{\mathbf{0}})\rangle_0} \\ &= \frac{e\lambda^2}{4\hbar^2}\int_{-\infty}^{\infty} dt'\,e^{i\omega_0t'}\left(\sum_{s=\pm} s\,e^{4\pi C_0(x_0,st';x_0,0)}\right), \end{aligned} \tag{A33}$$

where

$$C_0(x_0,t'';x_0,t') \,=\, \langle\Phi(\mathbf{r}''_{\mathbf{0}})\Phi(\mathbf{r}'_{\mathbf{0}})-\Phi^2(\mathbf{r}'_{\mathbf{0}})\rangle_0\,. \tag{A34}$$

One can thus see that I_0 and $I_{\rm BS}$ are actually independent of x and t, although the latter depends on the impurity position x_0.

APPENDIX B: CORRELATION FUNCTION

In this appendix, we derive an explicit expression for the correlation function of the Bose field of the ITLL model defined by the Hamiltonian (2).

We first observe that the field equation of motion obtained from Eq. (2) reads

$$\left(\frac{1}{v_F^2}\frac{\partial^2}{\partial t^2}-\frac{\partial}{\partial x}\frac{1}{g^2(x)}\frac{\partial}{\partial x}\right)\Phi(x,t) \,=\, 0\,. \tag{B1}$$

The solution can easily be found by determining the eigenfunctions of the inhomogeneous Laplacian, i.e., the x-dependent operator on the l.h.s. of (B1). Denoting by Λ the total length of the system (the wire plus the leads), and imposing periodic boundary conditions at $x=\pm\Lambda/2$ in the bulk of the leads, the above eigenfunctions fall into two groups, according to their parity (S=symmetric; A=antisymmetric), and read respectively

$$\psi_{S,k}(x)=\frac{1}{\sqrt{\Lambda}}\frac{1}{\sqrt{1+g^2-(1-g^2)\cos(kgL)}}\begin{cases}\sum_{s=\pm}(g+s)\cos\left[k(x-\frac{L}{2}(1-sg))\right] & x>\frac{L}{2}\\ 2g\cos(kgx) & |x|<\frac{L}{2}\\ \sum_{s=\pm}(g+s)\cos\left[k(x+\frac{L}{2}(1-sg))\right] & x<-\frac{L}{2}\end{cases} \tag{B2}$$

$$\psi_{A,k}(x)=\frac{1}{\sqrt{\Lambda}}\frac{1}{\sqrt{1+g^2+(1-g^2)\cos(kgL)}}\begin{cases}\sum_{s=\pm}\,s(g+s)\sin\left[k(x-\frac{L}{2}(1-sg))\right] & x>\frac{L}{2}\\ 2g\sin(kgx) & |x|<\frac{L}{2}\\ \sum_{s=\pm}\,s(g+s)\sin\left[k(x+\frac{L}{2}(1-sg))\right] & x<-\frac{L}{2}\end{cases} \tag{B3}$$

where $k\in]0;\infty[$ in the limit $\Lambda\to\infty$. The related (doubly degenerate) eigenvalue reads $E_k=\hbar\omega=\hbar v_Fk$.

The (non-time ordered) correlation function for the unperturbed system with Hamiltonian (2) can now easily be expressed in terms of these eigenfunctions[60], namely

$$\langle\Phi(x,t)\Phi(y,0)\rangle_0 = \sum_{b=S,A}\sum_{k>0}\frac{1}{2k}\psi_{b,k}(x)\psi_{b,k}(y)\left(e^{-i\omega t}+\frac{2\cos\omega t}{e^{\beta\hbar\omega}-1}\right). \tag{B4}$$

As usual in one dimension, the expression (B4) needs to be regularized, both in the infrared and ultraviolet regimes. In order to avoid the infrared divergency, we introduce the regularized correlation function

$$C_0(x,t;y,0) = \left\langle\Phi(x,t)\Phi(y,0)-\frac{\Phi^2(x,t)+\Phi^2(y,0)}{2}\right\rangle_0 \tag{B5}$$

and, in order to avoid the ultraviolet divergency, we mul-

tiply the r.h.s. of Eq. (B4) by $e^{-\omega/\omega_c}$, where the cut-off ω_c is related to the bandwidth.

From the knowledge of C_0 it is straightforward to compute the advanced, retarded and Keldysh Green functions, respectively, defined in Eqs. (A16)-(A17)-(A18), as well as their Fourier transforms

$$\tilde{\mathcal{C}}_0^a(x,y,\omega) = \int_{-\infty}^{\infty} e^{i\omega t}\, \mathcal{C}_0^a(x,t;y,0)\, dt \ , \tag{B6}$$

for $a = A, R, K$.

It is useful to separate the contributions to C_0 coming from the ground state (GS) and from thermal fluctuations (TF). Accordingly, we split the average value appearing in (B5) as $\langle \ldots \rangle = \langle \ldots \rangle_{\rm GS} + \langle : \ldots : \rangle$, where the symbols $\langle \ldots \rangle_{\rm GS}$ and $: :$ respectively indicate the average over the ground state of (2), and Boson normal ordering. Thus, we have

$$C_0 \ = \ C_{0;\rm GS} \ + \ C_{0;\rm TF} \ . \tag{B7}$$

As one can see from Eq. (B4), the temperature does not enter in the imaginary part of C_0, and therefore the conductivity $\sigma_0(x,y;\omega)$, related to C_0 through Eqs. (29), (B6), and (A17), is temperature independent. Below we explicitly give C_0 for x and y in the wire (i.e. $|x|, |y| \leq L/2$), because this is the case mostly needed in other sections.

$$\begin{aligned} &C_{0;\rm GS}(x,t;y,0) = \\ &-\frac{g}{4\pi}\left\{ \sum_{m\in Z_{\rm even}} \gamma^{|m|} \ln\left(\frac{(\alpha+i\tau)^2+(\xi_r+m)^2}{\alpha^2+m^2} \right) + \right. \\ &\left. + \sum_{m\in Z_{\rm odd}} \gamma^{|m|} \left\{ \ln\left(\frac{(\alpha+i\tau)^2+(m-\xi_R)^2}{\alpha^2+(m-\xi_R)^2} \right) + \frac{1}{2}\ln\left(\frac{[\alpha^2+(\xi_R+m)^2]^2}{[\alpha^2+(2\xi+m)^2]\,[\alpha^2+(2\eta+m)^2]} \right) \right\} \right\} , \end{aligned} \tag{B8}$$

$$\begin{aligned} &C_{0;\rm TF}(x,t;y,0) = \\ &-\frac{g}{4\pi}\left[\sum_{m\in Z_{\rm even}} \gamma^{|m|} \ln\left(\frac{|\Gamma[1+\Theta(\alpha+im)]|^4}{|\Gamma[1+\Theta(\alpha+i(\tau+\xi_r+m))]|^2\,|\Gamma[1+\Theta(\alpha+i(\tau-\xi_r-m))]|^2} \right) + \right. \\ &+ \sum_{m\in Z_{\rm odd}} \gamma^{|m|} \ln\left(\frac{|\Gamma[1+\Theta(\alpha+i(m-\xi_R))]|^4}{|\Gamma[1+\Theta(\alpha+i(\tau+m-\xi_R))]|^2\,|\Gamma[1+\Theta(\alpha+i(\tau-m+\xi_R))]|^2} \right) + \\ &\left. + \sum_{m\in Z_{\rm odd}} \gamma^{|m|} \ln \frac{|\Gamma[1+\Theta(\alpha+i(2\xi+m))]|^2\,|\Gamma[1+\Theta(\alpha+i(2\eta+m))]|^2}{|\Gamma[1+\Theta(\alpha+i(\xi_R+m))]|^4} \right] , \end{aligned} \tag{B9}$$

where $\xi = x/L$, $\eta = y/L$, $\tau = t\omega_L$, $\Theta = k_BT/\hbar\omega_L$, and $\alpha = \omega_L/\omega_c$ is the (dimensionless) inverse cut-off. As one can see, Eqs. (B8) and (B9) depend on time and temperature only through $t\omega_L$ and $k_BT/\hbar\omega_L$.

The part of the correlation function coming from thermal fluctuations does actually not need an ultraviolet cutoff, because the role of the cutoff is equivalently played by the finite temperature. Therefore, we can send $\alpha \to 0$ in Eq. (B9) and obtain the more familiar form

$$\begin{aligned} &C_{0;\rm TF}(x,t;y,0) = \\ &-\frac{g}{4\pi}\left[\sum_{m\in Z_{\rm even}} \gamma^{|m|} \sum_{r=\pm} \ln\left(\frac{\sinh\left[\pi\Theta(\tau+r(\xi_r+m))\right]}{\pi\Theta(\tau+r(\xi_r+m))} \frac{\pi\Theta m}{\sinh\left[\pi\Theta m\right]} \right) + \right. \\ &\left. + \sum_{m\in Z_{\rm odd}} \gamma^{|m|} \sum_{r=\pm} \ln\left(\frac{\sinh\left[\pi\Theta(\tau+r(m-\xi_R))\right]}{\pi\Theta(\tau+r(m-\xi_R))} \frac{\pi\Theta(m-\xi_R)}{\sinh\left[\pi\Theta(m-\xi_R)\right]} \right) + \right. \end{aligned}$$

$$+\sum_{m\in Z_{\rm odd}}\gamma^{|m|}\ln\left(\frac{\sinh^2\left[\pi\Theta(\xi_R+m)\right]}{\left[\pi\Theta(\xi_R+m)\right]^2}\frac{\pi\Theta(2\xi+m)}{\sinh\left[\pi\Theta(2\xi+m)\right]}\frac{\pi\Theta(2\eta+m)}{\sinh\left[\pi\Theta(2\eta+m)\right]}\right)\Bigg]\,, \tag{B10}$$

where we used the relation

$$|\Gamma[1+iX]|^2=\frac{\pi X}{\sinh\pi X}\,, \tag{B11}$$

which holds if X is real.

APPENDIX C: ASYMPTOTIC EXPANSION

In the present appendix, we provide the explicit expressions for the coefficients $D^{(1)}(\pm|\xi|;\Theta)$ and $D^{(2)}(\Theta)$ appearing in the asymptotic expansions (17) and (19). The former can be written as a product of a GS and a TF contribution

$$D^{(1)}(\pm|\xi|;\Theta)\,=\,D^{(1)}_{\rm GS}(\pm|\xi|)D^{(1)}_{\rm TF}(\pm|\xi|;\Theta)\,, \tag{C1}$$

where

$$\begin{aligned}D^{(1)}_{\rm GS}(\pm|\xi|)\;&=\;\left(\frac{4}{3\mp2|\xi|}\right)^{2g\gamma^2}\left(\frac{(9-4|\xi|^2)^2}{64(1\mp|\xi|)}\right)^{g\gamma^3}\\&\times\prod_{p=2}^{\infty}\left\{\left(\frac{(2p)^2}{(2p)^2-(1\mp2|\xi|)^2}\right)^{2g\gamma^{2p}}\prod_{r=\pm}\left(\frac{(2p+1+2r|\xi|)^2}{(2p+1+2r|\xi|)^2-(1\mp2|\xi|)^2}\right)^{g\gamma^{2p+1}}\right\}\end{aligned} \tag{C2}$$

and

$$\begin{aligned}D^{(1)}_{\rm TF}(\pm|\xi|;\Theta)\;&=\;\left(\frac{\pi\Theta(1\mp2|\xi|)]}{\sinh[\pi\Theta(1\mp2|\xi|)]}\right)^{2g}\prod_{p=1}^{\infty}\prod_{s=\pm}\left\{\left(\frac{\pi\Theta(1\mp2|\xi|+2ps)}{\sinh[\pi\Theta(1\mp2|\xi|+2ps)]}\frac{\sinh[\pi\Theta2p]}{\pi\Theta2p}\right)^{g\gamma^{2p}}\right.\\&\left.\times\prod_{r=\pm}\left(\frac{\pi\Theta(1\mp2|\xi|+s(2p-1+2r|\xi|))}{\sinh[\pi\Theta(1\mp2|\xi|+s(2p-1+2r|\xi|))]}\frac{\sinh[\pi\Theta(2p-1+2r|\xi|)]}{\pi\Theta(2p-1+2r|\xi|)}\right)^{g\gamma^{2p-1}}\right\}.\end{aligned} \tag{C3}$$

In Fig. 18, we have plotted $D^{(1)}(+|\xi|,\Theta)$ for $g=0.25$ as a function of the relative impurity position $|\xi_0|\in[0,1/2]$ and the temperature $\Theta=k_BT/\hbar\omega_L$, in the range $\Theta\in[0,1/2]$. Note that the expression (17) is by definition valid for $\Theta\ll1$ only. As one can see, the coefficient has a maximum at $\Theta=0$, which is of order 1. Similar values are also obtained for $D^{(1)}(-|\xi|,\Theta)$, and for other values of the interaction strength g.

The coefficient $D^{(2)}(\Theta)$ in Eq. (19) reads

$$D^{(2)}(\Theta)\,=\,D^{(2)}_{\rm GS}D^{(2)}_{\rm TF}(\Theta)\,, \tag{C4}$$

where

$$D^{(2)}_{\rm GS}\,=\,\prod_{m=2}^{\infty}\left(\frac{m^2}{m^2-1}\right)^{2g\gamma^{|m|}} \tag{C5}$$

and

$$D^{(2)}_{\rm TF}(\Theta)=\prod_{m=-\infty}^{\infty}\left(\frac{\pi\Theta(1+m)}{\sinh[\pi\Theta(1+m)]}\frac{\sinh[\pi\Theta m]}{\pi\Theta m}\right)^{2g\gamma^{|m|}}. \tag{C6}$$

This coefficient is shown in Fig. 19 for three different values of the interaction strength g.

APPENDIX D: LOCAL CONDUCTIVITY AND NOISE

The local conductivity is defined as

$$\sigma(x,y,\omega)=\int_{-\infty}^{+\infty}dt\;e^{i\omega t}\sigma(x,t;y,0), \tag{D1}$$

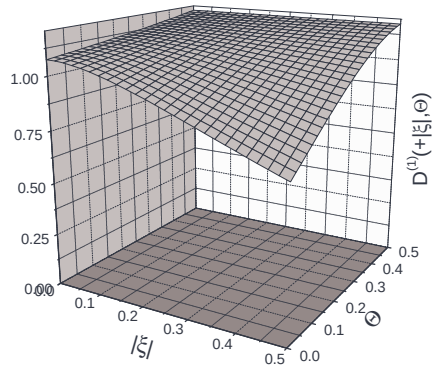

FIG. 18: The coefficient $D^{(1)}(+|\xi|,\Theta)$ as a function of the relative impurity position ξ and the dimensionless temperature $\Theta = k_B T/\hbar\omega_L$ for $g = 0.25$.

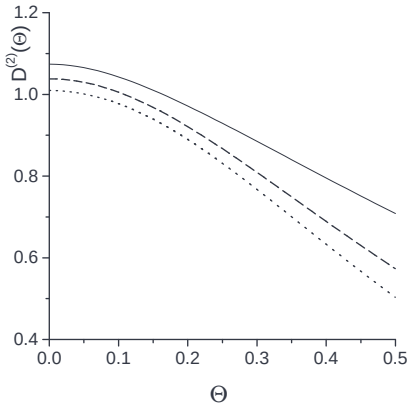

FIG. 19: The coefficient $D^{(2)}(\Theta)$ as a function of dimensionless temperature $\Theta = k_B T/\hbar\omega_L$ for $g = 0.25$ (solid line), $g = 0.5$ (dashed line), and $g = 0.75$ (dotted line).

where

$$\sigma(\mathbf{x};\mathbf{y}) = \left.\frac{\delta\langle j(\mathbf{x})\rangle}{\delta E(\mathbf{y})}\right|_{E=0} . \tag{D2}$$

Here, $\langle j(\mathbf{x})\rangle$ is given by Eq. (A28), and E is the external source appearing in the Hamiltonian (A3). Performing the functional derivative, and making use of the identity

$$\left\langle \frac{\delta^2\mathcal{H}_B}{\delta\Phi^2(\mathbf{r_0'})}[\Phi^\eta + A_0^\eta]\right\rangle_{\rightarrow} = \frac{i}{\hbar}\int_{-\infty}^{\infty} dt'' \sum_{\eta_2=\pm}\eta_2 \left\langle \frac{\delta\mathcal{H}_B}{\delta\Phi(\mathbf{r_0'})}[\Phi^\eta + A_0^\eta]\frac{\delta\mathcal{H}_B}{\delta\Phi(\mathbf{r_0''})}[\Phi^{\eta_2} + A_0^{\eta_2}]\right\rangle_{\rightarrow} , \tag{D3}$$

one easily obtains for the non-local conductivity

$$\sigma(x,y,\omega) = \sigma_0(x,y,\omega) - \frac{1}{2h\omega}\left(\frac{h}{e^2}\right)^2 \sigma_0(x,x_0,\omega)\sigma_0(x_0,y,\omega)\; f_C(x_0,\omega)|_{E=0} \ , \tag{D4}$$

where $\sigma_0(x,y,\omega)$ is given by Eqs. (29) and (B6), and f_C by Eq. (27).

The noise is computed starting from the expression

$$\langle\{\Phi(\mathbf{x}),\Phi(\mathbf{y})\}\rangle \;=\; \sum_{\eta,\eta'}\langle\frac{\Phi^\eta(\mathbf{x})\Phi^{\eta'}(\mathbf{y})}{2}\rangle$$

$$= \; -\left.\frac{\delta^2 Z[J]}{\delta J(\mathbf{x})\delta J(\mathbf{y})}\right|_{J=0} , \tag{D5}$$

which, using Eq. (A13), can be rewritten as

$$\langle\{\Phi(\mathbf{x}),\Phi(\mathbf{y})\}\rangle - 2\langle\Phi(\mathbf{x})\rangle\langle\Phi(\mathbf{y})\rangle = \sum_{a=0,B}\left(\frac{\delta Z_a}{\delta J(\mathbf{x})}\frac{\delta Z_a}{\delta J(\mathbf{y})} - \frac{\delta^2 Z_a}{\delta J(\mathbf{x})\delta J(\mathbf{y})}\right)\Big|_{J=0} . \quad \text{(D6)}$$

In particular, from Eq. (A19) we obtain

$$\frac{\delta Z_0}{\delta J(\mathbf{x})}\frac{\delta Z_0}{\delta J(\mathbf{y})} - \frac{\delta^2 Z_0}{\delta J(\mathbf{x})\delta J(\mathbf{y})}\Big|_{J=0} = \mathcal{C}_0^K(\mathbf{x};\mathbf{y}) , \quad \text{(D7)}$$

while the backscattering part (A20) gives

$$\begin{aligned}\frac{\delta^2 Z_B}{\delta J(\mathbf{x})\delta J(\mathbf{y})}\Big|_{J=0} &= \frac{i}{2\hbar}\int_{-\infty}^{\infty} dt' \sum_{\eta_1=\pm}\left(\eta_1\mathcal{C}_0^K + \mathcal{C}_0^R\right)(\mathbf{x};\mathbf{r}_\mathbf{0}')\left(\mathcal{C}_0^K + \eta_1\mathcal{C}_0^R\right)(\mathbf{y};\mathbf{r}_\mathbf{0}')\left\langle\frac{\delta^2\mathcal{H}_B}{\delta\Phi^2(\mathbf{r}_\mathbf{0}')}[\Phi^{\eta_1}+A_0]\right\rangle_{\rightarrow} \\ &+\frac{1}{2\hbar^2}\int_{-\infty}^{\infty} dt'\int_{-\infty}^{\infty} dt'' \sum_{\eta_1=\pm}\sum_{\eta_2=\pm}\left(\eta_1\mathcal{C}_0^K + \mathcal{C}_0^R\right)(\mathbf{x};\mathbf{r}_\mathbf{0}')\left(\eta_2\mathcal{C}_0^K + \mathcal{C}_0^R\right)(\mathbf{y};\mathbf{r}_\mathbf{0}'') \\ &\times\left\langle\frac{\delta\mathcal{H}_B}{\delta\Phi(\mathbf{r}_\mathbf{0}')}[\Phi^{\eta_1}+A_0]\frac{\delta\mathcal{H}_B}{\delta\Phi(\mathbf{r}_\mathbf{0}'')}[\Phi^{\eta_2}+A_0]\right\rangle_{\rightarrow} , \end{aligned} \quad \text{(D8)}$$

where $\mathbf{r}_\mathbf{0}'' = (x_0, t'')$. Observing that $\langle\frac{\delta^2\mathcal{H}_B}{\delta\Phi^2}[\Phi^\eta + A_0]\rangle_{\rightarrow}$ is independent of η, and exploiting the identity (D3), one obtains

$$\begin{aligned}\frac{\delta^2 Z_B}{\delta J(\mathbf{x})\delta J(\mathbf{y})}\Big|_{J=0} &= -\frac{1}{2e^2}\iint dt'dt'' \sum_{\eta_1,\eta_2=\pm}\left(\mathcal{C}_0^K(\mathbf{x};\mathbf{r}_\mathbf{0}')\mathcal{C}_0^R(\mathbf{y};\mathbf{r}_\mathbf{0}') + \mathcal{C}_0^R(\mathbf{x};\mathbf{r}_\mathbf{0}')\mathcal{C}_0^K(\mathbf{y};\mathbf{r}_\mathbf{0}')\right)\eta_2\langle j_B^{\eta_1}(\mathbf{r}_\mathbf{0}')j_B^{\eta_2}(\mathbf{r}_\mathbf{0}'')\rangle_{\rightarrow} \\ &+\frac{1}{2e^2}\iint dt'dt'' \sum_{\eta_1,\eta_2=\pm}\{\mathcal{C}_0^K(\mathbf{x};\mathbf{r}_\mathbf{0}')\mathcal{C}_0^R(\mathbf{y};\mathbf{r}_\mathbf{0}'')\,\eta_1\langle j_B^{\eta_1}(\mathbf{r}_\mathbf{0}')j_B^{\eta_2}(\mathbf{r}_\mathbf{0}'')\rangle_{\rightarrow} + \mathcal{C}_0^R(\mathbf{x};\mathbf{r}_\mathbf{0}')\mathcal{C}_0^K(\mathbf{y};\mathbf{r}_\mathbf{0}'')\,\eta_2\langle j_B^{\eta_1}(\mathbf{r}_\mathbf{0}')j_B^{\eta_2}(\mathbf{r}_\mathbf{0}'')\rangle_{\rightarrow} \\ &+\mathcal{C}_0^R(\mathbf{x};\mathbf{r}_\mathbf{0}')\mathcal{C}_0^R(\mathbf{y};\mathbf{r}_\mathbf{0}'')\,\langle j_B^{\eta_1}(\mathbf{r}_\mathbf{0}')j_B^{\eta_2}(\mathbf{r}_\mathbf{0}'')\rangle_{\rightarrow}\} . \end{aligned} \quad \text{(D9)}$$

Furthermore, we have

$$\frac{\delta Z_B}{\delta J(\mathbf{x})}\frac{\delta Z_B}{\delta J(\mathbf{y})}\Big|_{J=0} = \frac{2}{e^2}\iint dt'dt''\mathcal{C}_0^R(\mathbf{x};\mathbf{r}_\mathbf{0}')\mathcal{C}_0^R(\mathbf{y};\mathbf{r}_\mathbf{0}'')\,\langle j_B^\eta(\mathbf{r}_\mathbf{0}')\rangle_{\rightarrow}\langle j_B^\eta(\mathbf{r}_\mathbf{0}'')\rangle_{\rightarrow} . \quad \text{(D10)}$$

From the general definition (8) of the noise and the expression (7) for the current we obtain

$$S(x,y,\omega) = \frac{e^2}{\pi}\int_{-\infty}^{\infty} e^{i\omega t}\left(\langle\{\dot\Phi(x,t)\dot\Phi(y,0)\}\rangle - 2\langle\dot\Phi(x,t)\rangle\langle\dot\Phi(y,0)\rangle\right) . \quad \text{(D11)}$$

This formula for the noise can now be computed by inserting Eq. (D6) and using Eqs. (D7), (D9), and (D10). With the help of the relations

$$\sum_{\eta_1,\eta_2=\pm}\eta_1\,\langle j_B^{\eta_1}(\mathbf{r}')j_B^{\eta_2}(\mathbf{r}'')\rangle_{\rightarrow} = -2\theta(t''-t')\,\langle[j_B(\mathbf{r}'),j_B(\mathbf{r}'')]\rangle_{\rightarrow} ,$$

$$\sum_{\eta_1,\eta_2=\pm}\eta_2\,\langle j_B^{\eta_1}(\mathbf{r}')j_B^{\eta_2}(\mathbf{r}'')\rangle_{\rightarrow} = 2\theta(t'-t'')\,\langle[j_B(\mathbf{r}'),j_B(\mathbf{r}'')]\rangle_{\rightarrow} ,$$

$$\sum_{\eta_1,\eta_2=\pm}\langle j_B^{\eta_1}(\mathbf{r}')j_B^{\eta_2}(\mathbf{r}'')\rangle_{\rightarrow} = 2\,\langle\{j_B(\mathbf{r}'),j_B(\mathbf{r}'')\}\rangle_{\rightarrow} ,$$

and

$$\sum_{\eta_1,\eta_2=\pm}\eta_1\eta_2\,\langle j_B^{\eta_1}(\mathbf{r}')j_B^{\eta_2}(\mathbf{r}'')\rangle_{\rightarrow} = 0,$$

we derive the final result

$$S(x,y,\omega) = S_0(x,y,\omega) + S_A(x,y,\omega) + S_C(x,y,\omega) , \quad \text{(D12)}$$

where the three contributions to the FF noise read

$$S_0(x,y,\omega) = \frac{e^2\omega^2}{\pi}\tilde{\mathcal{C}}_0^K(x,y,\omega), \quad \text{(D13)}$$

$$S_A(x,y,\omega) = -\frac{\omega^2}{\pi}\tilde{\mathcal{C}}_0^R(x,x_0,\omega)\tilde{\mathcal{C}}_0^R(y,x_0,-\omega)f_A(x_0,\omega), \tag{D14}$$

and

$$S_C(x,y,\omega) = -\frac{\omega^2}{\pi}\left(\tilde{\mathcal{C}}_0^K(x,x_0,\omega)\tilde{\mathcal{C}}_0^R(y,x_0,-\omega)f_C(x_0,-\omega) + \tilde{\mathcal{C}}_0^R(x,x_0,\omega)\tilde{\mathcal{C}}_0^K(y,x_0,-\omega)f_C(x_0,\omega)\right) \quad . \tag{D15}$$

[1] S. Tarucha, T. Honda, and T. Saku, Solid State Comm. **94**, 413 (1995).
[2] A. Yacoby, H. L. Stormer, K. W. Baldwin, L. N. Pfeiffer, and K. W. West, Phys. Rev. Lett. **77**, 4612 (1996); Solid State Comm. **101**, 77 (1997).
[3] M. Bockrath, D. H. Cobden, J. Lu, A. G. Rinzler, R. E. Smalley, L. Balents, and P. L. McEuen, Nature **397**, 598 (1999).
[4] M. H. Devoret, D. Esteve, H. Grabert, G.-L. Ingold, H. Pothier, and C. Urbina, Phys. Rev. Lett. **64**, 1824 (1990).
[5] I. Safi and H. Saleur, Phys. Rev. Lett. **93**, 126602 (2004).
[6] W. Apel and T. M. Rice, Phys. Rev. B **26**, 7063 (1982).
[7] C. L. Kane and M. P. A. Fisher, Phys. Rev. B **46**, 1220 (1992).
[8] I. Safi and H. J. Schulz, Phys. Rev. B **52**, R17040 (1995).
[9] D. Maslov and M. Stone, Phys. Rev. B **52**, R5539 (1995).
[10] V. V. Ponomarenko, Phys. Rev. B **52**, R8666 (1995).
[11] I. Safi, Ann. Phys. (Paris) **22**, 463 (1997).
[12] I. Safi and H. J. Schulz, in *Quantum Transport in Semiconductor Submicron Structures*, edited by B. Kramer (Kluwer Academic Press, Dordrecht, 1995).
[13] A. Furusaki and N. Nagaosa, Phys. Rev. B **54**, R5239 (1996).
[14] N. P. Sandler, C. de C. Chamon, and E. Fradkin, Phys. Rev. B **57**, 12324 (1998).
[15] A. V. Lebedev, A. Crépieux, and T. Martin, cond-mat/0405325
[16] M. Fabrizio and A. O. Gogolin, Phys. Rev. B **51**, 17827 (1995).
[17] R. Egger and H. Grabert, Phys. Rev. Lett. **77**, 538 (1996).
[18] R. Egger and H. Grabert, Phys. Rev. B **58**, 10761 (1998).
[19] R. Egger, H. Grabert, A.Koutouza, H. Saleur, and F. Siano, Phys. Rev. Lett. **84**, 3682 (2000).
[20] I. Safi, Eur. Phys. J. B **12**, 451 (1999).
[21] K.-V. Pham, Eur. Phys. J. B **36**, 607 (2003).
[22] F. Dolcini, H. Grabert, I. Safi, and B. Trauzettel, Phys. Rev. Lett. **91**, 266402 (2003).
[23] Y. M. Blanter and M. Büttiker, Phys. Rep. **336**, 1 (2000).
[24] C. de C. Chamon, D. E. Freed, and X. G. Wen, Phys. Rev. B **53**, 4033 (1996).
[25] Y. M. Blanter, F. Hekking, and M. Büttiker, Phys. Rev. Lett. **81**, 1749 (1998).
[26] V. V. Ponomarenko and N. Nagaosa, Phys. Rev. B **60**, 16865 (1999).
[27] B. Trauzettel, R. Egger, and H. Grabert, Phys. Rev. Lett. **88**, 116401 (2002).
[28] C. L. Kane and M. P. A. Fisher, Phys. Rev. Lett. **72**, 724 (1994).
[29] R. de Picciotto, M. Reznikov, M. Heiblum, V. Umansky, G. Bunin, and D. Mahalu, Nature **389**, 162 (1997).
[30] L. Saminadayar, D. C. Glattli, Y. Jin, and B. Etienne, Phys. Rev. Lett. **79**, 2526 (1997).
[31] B. Trauzettel, I. Safi, F. Dolcini, and H. Grabert, Phys. Rev. Lett. **92**, 226405 (2004).
[32] C. Bena, S. Vishveshwara, L. Balents and M.P.A. Fisher, J. Stat. Phys. **103**, 429 (2001).
[33] R. Deblock, E. Onac, L. Gurevich, and L. P. Kouwenhoven, Science **301**, 203 (2003).
[34] R. J. Schoelkopf, P. J. Burke, A. A. Kozhevnikov, D. E. Prober, and M. J. Rooks, Phys. Rev. Lett. **78**, 3370 (1997).
[35] P.-E. Roche, M. Kociak, S. Gueron, A. Kasumov, B. Reulets, and H. Bouchiat, Eur. Phys. J. B **28**, 217 (2002).
[36] N. Y. Kim, W. D. Oliver, Y. Yamamoto, J. Kong, and H. Dai, cond-mat/0311434.
[37] F. D. M. Haldane, J. Phys. C: Solid State Phys. **14**, 2585 (1981).
[38] J. Nygård, D. H. Cobden and P. E. Lindelof, Nature **408**, 342 (2000).
[39] J. Kong, E. Yenilmez, T. W. Tombler, W. Kim, H. Dai, R. B. Laughlin, L. Liu, C. S. Jayanthi, and S. Y. Wu, Phys. Rev. Lett. **87** 106801 (2001).
[40] W. Liang, M. Bockrath, D. Bozovic, J. H. Hafner, M. Tinkham, and H. Park, Nature **411**, 665 (2001).
[41] T. Kleimann, F. Cavaliere, M. Sassetti and B. Kramer, Phys. Rev. B **66**, 165311 (2002).
[42] W. Häusler, L. Kecke, and A. H. MacDonald, Phys. Rev. B **65**, 085104 (2002).
[43] V. V. Ponomarenko and N. Nagaosa, Phys. Rev. B **56**, R12756 (1997).
[44] C. L. Kane and M. P. A. Fisher, Phys. Rev. B **67**, 045307 (2003).
[45] This can, for instance, be seen from Eq. (A22). If the correlation function of the homogenous TLL were used instead of $i\mathcal{C}_0^R(\mathbf{r};\mathbf{x})$, the result of Eq. (A31) would have a prefactor g in front of it. Essentially, the homogeneous TLL performes the time-integral in Eq. (A22) over times that are always smaller than the traversal time ω_L^{-1} of the wire, whereas the ITLL does not include such a restriction.
[46] V. V. Ponomarenko, Phys. Rev. B **54**, 10328 (1996).
[47] B. Trauzettel and H. Grabert, Phys. Rev. B **67**, 245101 (2003).
[48] C. Chamon and D. E. Freed, Phys. Rev. B **60**, 1842 (1999).
[49] F. Lesage and H. Saleur, Nucl. Phys. B **490**, 543 (1997).
[50] L. S. Levitov and G. B. Lesovik, JETP Lett. **58**, 230 (1993); G. B. Lesovik and R. Loosen, JETP Lett. **65**, 295 (1997).

[51] M. P. A. Fisher and L. I. Glazman in *Mesoscopic Electron Transport*, Vol. 345 of NATO ASI, edited by L. Kouwenhoven, G. Schön, and L. Sohn (Kluwer, Dordrecht, 1997).
[52] K.-V. Pham, M. Gabay, and P. Lederer, Phys. Rev. B **61**, 16397 (2000).
[53] Although the period of the function $F(\omega)$ in Eq. (56) is $2\pi\omega_L = 2\Delta\omega_1$, by virtue of the symmetry of $F(\omega)$ around $\omega = \pi\omega_L$ (see Fig. 14), an averaging over half the period is sufficient to obtain the result in Eq. (57).
[54] B. Reulet, J. Senzier, and D. E. Prober, Phys. Rev. Lett. **91**, 196601 (2003).
[55] C. S. Peca, L. Balents, and K. J. Wiese, Phys. Rev. B **68**, 205423 (2003).
[56] S. G. Lemay, J. W. Janssen, M. van den Hout, M. Mooij, M. J. Bronikowski, P. A. Willis, R. E. Smalley, L. P. Kouwenhoven, and C. Dekker, Nature **412**, 617 (2001).
[57] Y. Tserkovnyak, B. I. Halperin, O. M. Auslaender, and A. Yacoby, Phys. Rev. B **68**, 125312 (2003).
[58] B. Gao, A. Komnik, R. Egger, D. C. Glattli, and A. Bachtold, Phys. Rev. Lett. **92**, 216804 (2004).
[59] L. V. Keldysh, Zh. Eksp. Teor. Fiz. **47**, 1515 (1964) [Sov. Phys. JETP **20**, 1018 (1965)]; H. Kleinert, *Path Integrals in Quantum Mechanics, Statistics, and Polymer Physics* (World Scientific, Singapore, 1995).
[60] E. N. Economou, *Green's Functions in Quantum Physics* (Springer-Verlag, Heidelberg, 1983).